APPLICATION OF PHOTOGRAMMETRIC AND REMOTESENSING METHODS FOR IDENTIFICATION OF RESISTANCE COEFFICIENTS OF HIGH WATER FLOW IN RIVER VALLEYS

Przemysław Tymków

APPLICATION OF PHOTOGRAMMETRIC AND REMOTESENSING METHODS FOR IDENTIFICATION OF RESISTANCE COEFFICIENTS OF HIGH WATER FLOW IN RIVER VALLEYS

UWP

Contents

Index

Introduction

When considering a river valley during the passing of the flood wave as a physical system, it is necessary to determine the state of this system, its characteristic variables and its response to the external factors. A mathematical abstraction is modelled to determine the features of this physical system. Due to the role of the floodplains in farming as well as the flood consequences, flow modelling in valleys is an important part of hydromechanics and hydraulics. Publications on determination of flood hazard zones and the methods to limit flood consequences have became particularly important after the floods of 1997 and 1998 (Kubrak and Nachlik, 2003; Radczuk et al., 2001; Grocki and Czamara, 2001).

The river valley as a floodplain features high diversification of land cover which influences surface roughness to a great extent. In particular, valleys which are used for farming (arable lands, meadows and pastures), small plants (shrubs) and tall plants (clump of trees, forests) have different flow resistance. Parameterization of selected geometric features of plants depends on establishing the type of plants (particularly in case of tall plants − deciduous trees, coniferous trees) and their height (Mokwa, 2003). The knowledge of these parameters facilitates evaluation of characteristic data for the surface roughness classes such as spacing of trees, diameters of trunks, etc. In hydrodynamic calculations, the value of resistance coefficient can be established on the basis of calculations which tare the model (Parzonka et al., 2000). It requires, inter alia, hydrodynamic measurements of hydraulic parameters (velocity distribution in section), which is not always possible in the case of a passing flood wave. The other approach depends on determination roughness coefficients on the basis of the shape and land cover analysis. Maps, aerial photographs, GIS databases and site surveys results are used for this purpose. The most common method of identification and classification of images in the aerial photographs is a visual interpretation, called photointerpretation (Ciołkosz et al., 1999). The development of new measurement techniques such as laser scanning and advanced digital methods of classification, e.g. neural networks, may be the basis to claim that these methods can be used to assess the forms of land cover on floodplains with allowance for flow coefficients.

This paper is the result of a research which has been carried out over the course of a few years and which focused on remote sensing, photogrammetric, digital acquisition and digital processing methods for the purpose of surface roughness evaluation of floodplains. It presents the technique of automatic identification of land cover for the need of evaluation of resistance coefficients of flood waters on

the floodplains using the method of computer-aided decision making and transformation of the obtained coefficients to a hydrodynamic model. Chapter 1 of this publication is an attempt to summarize the literature concerning issues of hydrodynamic calculations and determination of flood hazard zones with respect to the role and methods of flow resistance evaluation. Due to the purpose and nature of this publication, this knowledge is crucial to learn and understand the needs of experts who work in this field. Chapter 2 concerns classification in remote sensing, particularly new techniques and solutions. A method of automatic identification of land cover classes for the need of hydraulic features evaluation of floodplains is also discussed here. The potential sources of data for this classification and the accepted method of accuracy assessment were also indicated. Chapter 3 provides a description of the adopted identification method in the selected part of the river valley, short description of the study area, a discussion of possible approaches to classification as well as an analysis of the results obtained and their accuracy evaluation. Chapter 4 is a summary.

Chapter 1

The role of flow resistance coefficients in hydraulic calculations of natural open river beds

Hydraulic calculations of flow parameters in natural open river-beds have been extensively discussed in the existing professional literature (Kubrak and Nachlik, 2003; Sobota, 1994; Puzyrewski and Sawicki, 2000; Nachlik, 2000; Dąbkowski and Pachuta, 1996). Due to the diversified shapes of flow areas, as well as forms of land cover, the rising discharges which frequently extend to economically exploited areas, present a difficult issue to study. A correct determination of hydraulic characteristics of high water in river valleys requires the estimation of parameters which describe the flow resistance. While the roughness parameters of the majority of material types which may compose the bottom and sidewalls of river-beds (especially the ones that can not be washed away) have already been precisely determined and tabled (Chow, 1959), the estimation of the influence of plants on the flow capacity of river-beds and valleys is a problematic issue, mostly due to the richness of plant types and the dynamic changes of plants features (Tymiński, 1996). The occurrence of plants on floodplains of river beds intensifies the interchange of water masses between the floodplain and the main river bed. The phenomenon applies mostly to tall plants (taller than the flow depth and unlikely to change under the influence of the hydrodynamic water pressure (Bretschneider and Schultz, 1985)) and is called interaction. It impedes the water flow in the river-bed and is very important for determining the rising discharge flow in river valleys and for specifying the flood-threatened areas (Nachlik, 2000).

1.1. Estimation of flow resistance in floodplains

A number of technical problems concerning the flow capacity of river beds are solved by the assumption that the water flow in a river bed is fixed and uniform. Although the aforementioned assumptions are valid for numerous cases, they are also erroneously used in situations in which not all of the conditions are fulfilled (a situation of water flow obstructed by plants may be an example). When the water flow is obstructed by tall plants (trees), the flow is regarded as quasi-uniform (Kubrak and Nachlik, 2003). One of the most fundamental formulas in the study of hydraulics of open river-beds is the Chézy formula, describing the mean flow velocity of steady, turbulent open channel flow:

$$\nu = C\sqrt{RJ} \tag{1.1}$$

where: ν − mean velocity of water flow in the cross-section,
             C − Chézy resistance coefficient,
             R − hydraulic radius of the cross-section,
             which can be expressed in the form of the following equation:

$$R = \frac{A}{O} \tag{1.2}$$

where: A − cross-sectional area of the flow,
             O − wetted perimeter.
             J − hydraulic gradient (the fall of the energy line
             in the uniform motion, which is equal to the bottom fall).

The mean velocity of water flow can also be calculated on the basis of empirical dependencies presented by:
— Strickler (Sobota, 1994):

$$\nu = k_{st} R^{\frac{2}{3}} J^{\frac{1}{2}} \tag{1.3}$$

    where: k_{st} − roughness coefficient of the bottom surface and sidewalls.

— Manning (Sobota, 1994; Puzyrewski and Sawicki, 2000):

$$\nu = \frac{1}{n} R^{\frac{2}{3}} J^{\frac{1}{2}} \tag{1.4}$$

    where: n − roughness coefficient of the bottom surface and sidewalls.

Analysis of formulas 1.1, 1.3 and 1.4 leads to the derivation of an equation illustrating the dependencies between various coefficients which characterize the river bottom and sidewalls resistance:

$$C = k_{st} R^{\frac{1}{6}} \tag{1.5}$$

$$k_{st} = \frac{1}{n} \tag{1.6}$$

An extensive collection of numerical values for the C, k_{st} and n coefficients, as well as for various surface types is presented in the professional literature (Sobota, 1994; Kubrak and Nachlik, 2003; Puzyrewski and Sawicki, 2000).
The flow resistance can also be calculated on the basis of the universal Darcy-Weisbach equation, by establishing the value of the coefficient λ (Sobota, 1994):

$$\nu = \sqrt{\frac{8gRJ}{\lambda}} \tag{1.7}$$

where: g − gravitational acceleration,
             λ − linear resistance coefficient.

The λ coefficient for uniform surface roughness can also be established (while making certain assumptions) on the basis of the simplified Colebrook-White equation:

$$\lambda = \left[-2.0 \log \left(\frac{k_s}{14.84R} \right) \right]^{-2} \tag{1.8}$$

where: k_s − absolute river-bed roughness.

The relation between n, k_{st} coefficients and the non-dimensional λ coefficient is given by the following equation:

$$k_{st} = \frac{1}{n} = \sqrt{\frac{8gRJ}{\lambda R^{\frac{1}{3}}}} \tag{1.9}$$

The use of n or λ coefficient in mathematical modelling depends on the employed computer software, which is based on one of the possible methods of flow resistance calculations (Kubrak and Nachlik, 2003). In the contemporary, high-quality computer software the motion resistance is mostly determined on the basis of a generalized flow law. It is most frequently applied to the studies of areas covered by plants, where the surface and vegetation parameters determine the strength of motion resistance. The problems of growth parameterization and related flow calculations have been widely discussed in the papers by Kałuża (1996, 1999, 1995a,b), Kubrak and Nachlik (2003), Żelazo (2002) and Rickert (1986). Other authors, e.g. Petryk and Bosmajian (1975), Kouwen and Unny (1973), Dąbkowski and Pachuta (1996), Tymiński (1996) studied the influence of various types of plants on the water flow resistance and usually proposed their own formulas related with the average numerical values of the plants geometrical parameters. It is important to bear in mind that the character of plant flow resistance change with the velocity of water flow. According to The German Association of Water Management and Land Melioration the description of vegetation from the point of view of hydraulic calculations should include the type, distribution and arrangement of existing plants (Parey, 1991). In practice, the plants are grouped on the basis of hydraulic criteria into (Kałuża, 1996):
— dense groups of trees or shrubs,
— single trees or shrubs,
— mixtures of trees and shrubs.

The flow resistance of tall plants depends mostly on the resistance of the plant's bulk shape, which is flown around by water. In case of a clump of trees, the parameterization of the plants is reduced to establishing their average diameter d_p and spacing a_x and a_y (Fig. 1.1). The coefficient of a clump of trees λ_p is given by:

$$\lambda_p = C_{WR} \frac{4d_p h \cos \alpha}{a_x a_y}, \tag{1.10}$$

where: h − depth of the flow,
α − inclination angle of the area's longitudinal profile.

The resistance coefficient of the water flow for a clump of trees C_{WR} is given by Rickert (Rickert, 1986):

$$C_{WR} = \left[1.1 + 2.3\frac{d_p}{a_y}\right] \cdot \left[0.6 + 0.5\log\left(\frac{a_x}{a_y}\right)\right] + 2 \cdot \left[\frac{1}{1 - \frac{d_p}{a_y}} - 1\right] \qquad (1.11)$$
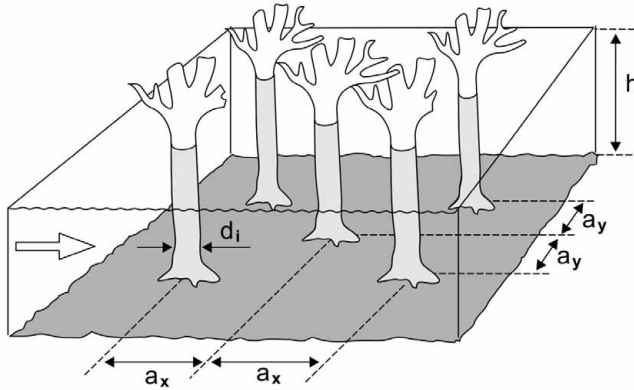
Figure 1.1. Parameterization of geometrical features of tall plants.

The resistance coefficient for shrubs may be established similarly (Kałuża, 1999), with only one difference: in case of areas overgrown by single shrubs, a_x, a_y, d_p are treated as macro-structural dimensions, that is the spacing and diameter of an entire shrub (here, shrubs are perceived as impermeable objects), while the micro-structural model is applied to areas densely overgrown by shrubs (here, plants are treated as permeable and the average diameter d_p and spacing a_x, a_y of branches play an important role). The flow resistance coefficient accepted for calculations is a sum of the trees (shrubs) resistance coefficient λ_p and the river bottom resistance coefficient λ_d (Kubrak and Nachlik, 2003):

$$\lambda = \lambda_p + \lambda_d \qquad (1.12)$$

Specification of the plants substitute parameters requires that the measurement is conducted on representative areas, called sample plots (Kukuła et al., 1997). Due to the vastness of the floodplains, a comprehensive recording of existing vegetation is impossible. Numerous authors have suggested using the statistical method to record the vegetation. The method implies drawing conclusions concerning the parameters of the entire area on the basis of a statistical sample. **The method proposed in the presented paper is based on a direct recording of vegetation on sample plots, and then preparing a feature vector that describes**

the plots and is followed by an attempt to locate similar plots on the entire study area by conducting a supervised classification.

1.2. Hydrodynamic modeling as a tool for flood protection

The notion of flood is understood as a set of complex phenomena and conditions that accompany freshets and eolian water lifting and water rising due to river congestion occurring at inland waterways and maritime belt, and causing security threat, as well as economic, social and moral losses (Radczuk et al., 2001). According to the methodology of (Nachlik, 2000), the study of flood threat should encompass the evaluation of the existing flood protection system, based on inventory control of flood protection facilities, river-bed evaluation from the point of view of water discharge, and the evaluation of the condition of river banks and water discharge facilities on built-up areas. The evaluation of a river-bed capacity of water discharge can partially be based on hydraulic calculations that include information concerning the shape and development of the studied area. Topographic data can be represented as formulas, boundary conditions and coefficients (for instance, related to roughness). The geometry and land development are usually defined on the basis of through, geodetic site surveys and, more frequently nowadays, via remote methods (Photogrammetry and Remote Sensing) (Gołuch et al., 2000, 2004).

The increasing accuracy and detail of river-beds descriptions, related to improved data acquisition and processing methods, allow implementatin of advanced mathematical models that simulate water flow processes.

1.2.1. Computer simulation of river water flow

Difficulties related to simulation of various physical processes with real hydraulic models led to the development of mathematical modeling (Majewski, 2005). A mathematical model of a river stretch is a certain mathematical abstraction, which is related to variables characterizing the state of a system, external impact on that system and its reactions to this impact, being always a simplification of the real system where the complexity is practically unlimited (Radczuk et al., 2001). As the ratios of river lengths to their widths and depths are usually incomparable, first one dimensional (1D) model systems were invented and implemented. There, the distribution of velocity and other values, e.g. temperature, changes in only one direction which is the direction of water flow. Although such approach is very simplistic, in most cases it can be successfully employed by engineers (Majewski, 2005). Due to the increasing computational capacities of computers, numerical, two-dimensional modeling of open river-beds became possible. Physical parameters in such models are averaged in the vertical direction but they change horizontally. Attempts have been made to employ three-dimensional models in hydraulic calculations, but the great number of data required for model calibration, as well as

the task's computational complexity prohibited their use by engineers (Majewski, 2005).

A number of computer systems employed to hydrodynamic modeling have been developed, e.g.: HEC-RAS, HEC-HMS (developed by US Army Corps of Engineers - Hydraulic Engineering Center), MIKE 11, MIKE 21 (Danish Hydraulic Institute), SMS (Brigham Young University), CARIMA (Laboratoire d'Hydraulique de France), FLUVIAL National Research Council USA) and SiReN (Wrocław University of Environmental and Life Sciences).

1.2.2. Means of surface roughness representation in hydrodynamic models

Depending on the employed approach and type of hydraulic calculations, the surface roughness can be described in various ways. Researchers (Sobota, 1994; Radczuk et al., 2001; Kubrak and Nachlik, 2003) emphasize the importance of a proper surface roughness estimation for correct water flow calculation. This applies to both: river beds (which is not the subject of this paper) and floodplains, that are particularly relevant for the issues of high water flow calculations and modeling).

Depending on the number of coordinates required for water flow description, the computer systems used for hydrodynamic phenomena modeling are classified as follows: one-dimensional (1D), two-dimensional (2D) and three-dimensional (3D).

One-dimensional models (1D)

One-dimensional systems, which are based on the assumption that the velocity component is in agreement with the river axis direction, employ description of the flow area geometry in the shape of cross-sections perpendicular to the direction of the river flow (HEC-RAS, 2006). *HEC-RAS* computer program is an example of 1D system developed by US Army Corps of Engineers. It is based on the *Muskingum* and *Muskingum-Cunge* kinematic wave model (Kot and Szymkiewicz, 2002), and the calculations are made from one cross-section to the next by solving a fixed multivariant flow equation using the iteration method. Determination of velocity coefficients for a single cross-section involves the division of a flow area into parts that have identical properties. Two approaches to the problem of roughness description in one-dimensional models prevail (Radczuk et al., 2001):

— acceptance of a substitute coefficient for a river-bed and each floodplain separately, avoiding the division into smaller zones,
— acceptance of a substitute coefficient for a river-bed exclusively, while the floodplains section is divided into parts, each of which is treated as a compact section, homogenous from the point of view of their roughness.

Both of the described approaches can be employed in the *HEC-RAS* system. Most often, however, the river-bed area is treated as an indivisible element, while the surrounding lands are divided into parts on the basis of establishing points of
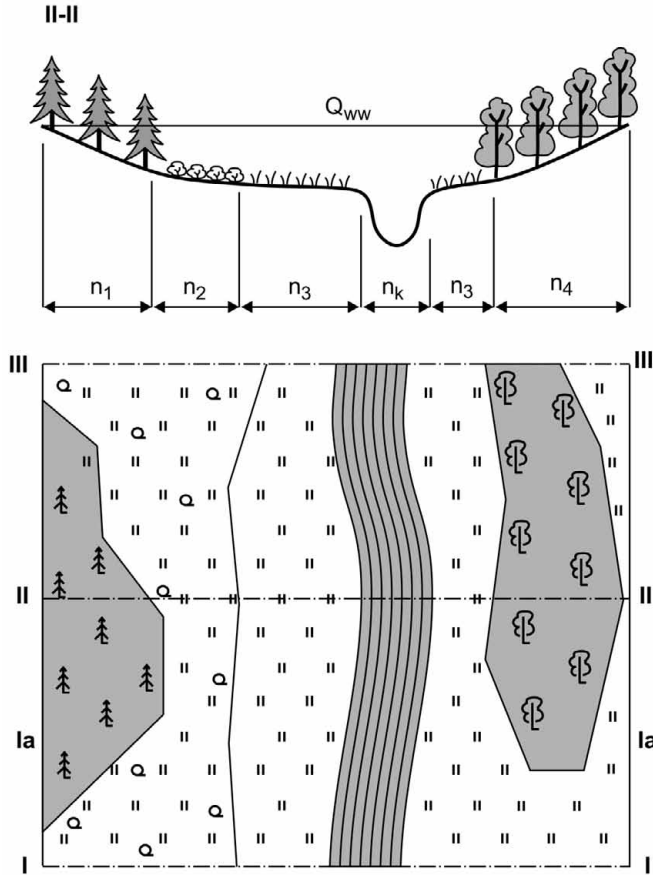
Figure 1.2. Surface roughness representation in 1D models (Mokwa, 2003)

change in the roughness coefficient, according to Manning formula (1.4) (Sobota, 1994). This is illustrated in Fig. 1.2.

The value of the roughness coefficient on a segment cross-section should make allowance not only for the change in surface hydraulic properties along the cross-section, but also of the whole area till the next cross-section. The means of mapping floodplain roughness coefficient on a calculation cross-section are described in (Gierczak, 1998). On the basis of the methods described by Gierczak, three general approaches to the problem can be distinguished: the first one concerns to the roughness expressed in segments on a cross-section, while the other two concern the substitute roughness for the entire floodplain. The first method is based on the division of the right and left floodplain cross-section into segments,
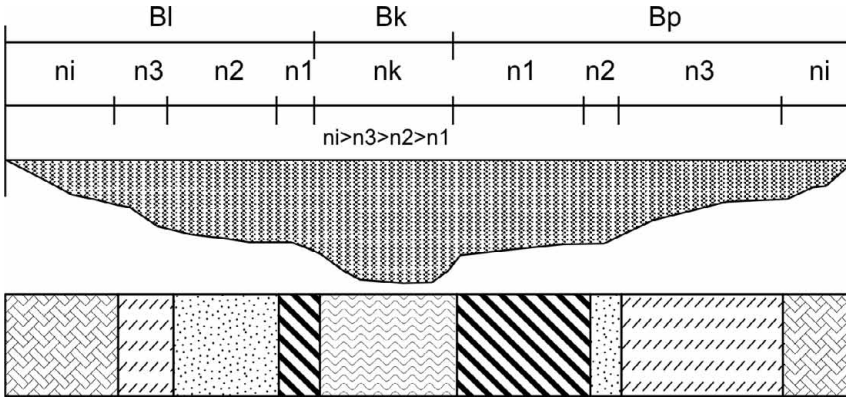
Figure 1.3. Scheme of the method for roughness calculation in a cross-section
(Gierczak, 1998)

each of which possesses its own distinguishable properties. The division reflects the
percentage share of a partial area F_i in the entire area, according to the formula
(Gierczak, 1998):

$$L_i = \frac{F_i}{\sum_{i=1}^{n} Fi} \cdot B, \tag{1.13}$$

where: L_i − i-th cross-section segment,
          B − roughness of the floodplain.

According to the presented method, segments are arranged along the cross-section
in such a way that the rougher segments are located at the external valley-banks,
while the segments of smaller roughness value are located at the river-bed (vide:
Fig. 1.3).

   The second and third method require the calculation of the substitute coeffi-
cient as the average roughness from partial areas. The way of defining the average
distinguishes the two methods. In practice, however, expression of a coefficient ac-
cording to the changes observed along the cross-section is usually employed. The
method is legitimate when the cross-sections are made frequently and in places
characteristic from the point of view of their shape and roughness changes.

   Two-dimensional models (2D)

Two-dimensional models are employed to simulate water flow in river-beds where
the vertical vector components of velocity and acceleration are considerably smaller
than their components in the horizontal plane. *RMA2* from the *SMS* package
may be an example of such a model. It is used for modeling water flow and trans-
port of particles in rivers, estuaries and coastal belts. The package employs the
finite-element method in order to solve equations which describe two-dimensional
water flow and depositional transport. It also allows for one-dimensional cal-
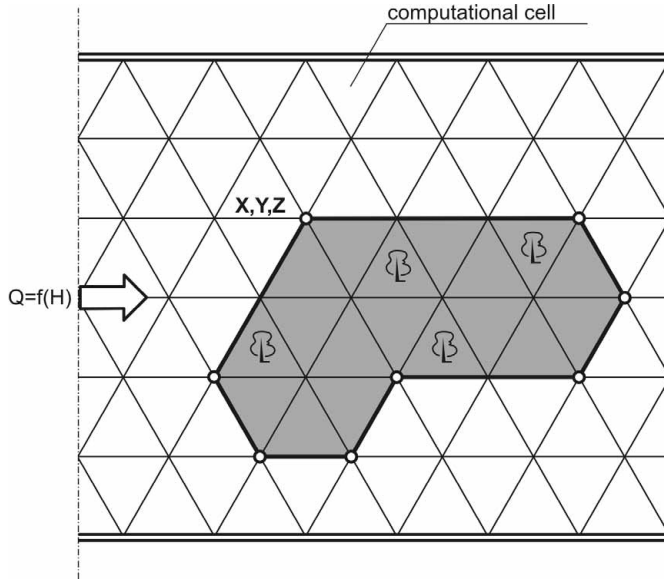
Figure 1.4. Scheme of the method for roughness representation in 2D models (Mokwa, 2003)

culations in cases when two-dimensional calculations are not required, and for three-dimensional calculations in special situations. The velocity components − averaged vertically − in the horizontal plane are calculated by integration of a three-dimensional set of equations of conservation of mass and momentum along the vertical component from the bottom to the water surface. It is assumed that the movement along the vertical component is irrelevant and the constant water density is ρ. Solution of the equations requires establishing a number of parameters which describe hydraulic and geometric properties of the modeled area. According to (Froehlich, 2002), description of river-bed and flood-plain roughness characteristics should be based on site surveys (this is particularly important for a river-bed), as well as aerial photographs, ground photographs and topographic maps. Information concerning the surface roughness is often saved together with information concerning relief in the form of a digital terrain model (Fig. 1.4). The majority of the computer systems used for water flow modeling can use data gathered in the Geographic Information Systems (GIS). It is, therefore, possible to use the same information concerning the layout of the land (usually in the form of digital terrain model) and its forms of covering in the majority of systems as a thematic layers, and − by means of appropriate tools − to transform those values into the form required by a model.

Chapter 2

Supervised classification of land cover as a method of surface roughness evaluation on flood-plains

The characteristic parameters of plants are defined on the basis of inventory and direct site surveys (Kubrak and Nachlik, 2003). Detailed determination of plant types and estimation of d_p, a_x and a_y geometric parameters of tall plants (chapter 1.1) require labor intensive studies and site inspections. Application of modern techniques of remote sensing and aerial photographs allows estimation of those parameters with little or no field work involved, especially in cases when a visual analysis of trees, based on oblique aerial photographs is supplemented by the information concerning tree height. First, an expert defines the properties of plants on small test fields and then − by means of a statistic or computer aided decision method (which is the subject of the present work) − he identifies similar areas occurring in the entire study area. The method can also be used to determine other forms of land cover and to assign resistance parameters to them, which is a much easier task. a map of areas of similar roughness parameters, which was created in this process, may, next to the numerical terrain model, serve for both one and two-dimensional hydrodynamic modeling (Mokwa and Tymków, 2004; Tymków and Mokwa, 2005; Tymków et al., 2006).

2.1. Theoretical basis of the recognition problem

The ability to recognize objects (phenomena, processes, signals, situations) can be defined as the ability to assign them a definite meaning (class) on the basis of their certain characteristic properties (features) (Kurzyński, 1997). In order to recognize an object correctly, measurements and a correct selection of features are necessary. These tasks constitute separate problems in the recognition process. Measurable values of features (for instance: from continuous or discrete domain of real numbers, natural numbers or fuzzy numbers) put together in one column are called feature vectors:

$$\mathsf{x} = \begin{bmatrix} x^{(1)} \\ x^{(2)} \\ \vdots \\ x^{(d)} \end{bmatrix} \tag{2.1}$$

The feature vector constitutes a source of information about a classified object for recognition algorithms and methods. Two main stages can be distinguished in the recognition process (Hoppner et al., 1999; Tadeusiewicz, 1993; Linh, 2004; Kurzyński, 1997):

— measurement, selection and reduction of features describing the classified object,

— proper classification on the basis of feature vector.

In order to accomplish classification in X feature space, which is for the assumption $x \in R$ a multidimensional sub-space of the Euclidean space ($X \subseteq R^n$), features of objects from the same class should be located close to one another in the sense of the Euclidean geometry (feature variation should be small (Linh, 2004), but at the same time they should be separated from the clumps of points from other classes (Tadeusiewicz and Flasiński, 1991; Kurzyński, 1997). This rule, known in the literature (Tadeusiewicz and Flasiński, 1991) as the Brawermann's rule, constitutes the basic law, on the basis of which it is possible to distinguish one object from another. As in the majority of tasks the number of features that can be gained is very large, their increasing number in all of the algorithms leading to considerable computational complication of the task, it is important to limit the size of the feature vector to a minimum that still guarantees proper recognition. This activity, known as feature selection, should precede the task of classification, but its nature is very complex, often heuristic and arbitrary. When the number of all the object features (N) exceeds considerably the number of features that can be used in the classification process (d), it is possible to talk about a special task of discrete optimization in which the set of possible solutions equals:

$$\left(\begin{array}{c} n \\ k \end{array} \right) = \frac{N!}{d! \, (N - d)!} \tag{2.2}$$

Solution of this problem is not easy, and the impossibility of its algoritmization compels numerous authors to offer various optimization methods (for instance based on neural networks, genetic algorithms, etc.) for solving it (Meyer-Bäse, 2004; Tadeusiewicz, 1993; Cichocki and Unbehauen, 2002; Vonk et al., 1997). The proper classification means that each $x \in X$ vector is assigned to a $i \in M$ class number, where $M = \{1, 2, \ldots, m\}$, by means of certain Ψ decision rule, called a classification algorithm:

$$\Psi : X \to M \tag{2.3}$$

Realization of an algorithm is called a classifier.

In general, all the classification methods can be divided into unsupervised methods (without a trainer) and supervised methods (with a trainer) (Meyer-Bäse, 2004; Kurzyński, 1997; Cichosz, 2000; Kwiatkowski, 2001; Adamczyk and Będkowski, 2005; Mularz, 2004).

Supervised classification

The construction of a classifier, that allows for the class themes required by the

user, is based on certain knowledge obtained from external sources (from the so-called expert or on the basis of the S_j training sequence) (Campbell, 1996; Kurzyński, 1997; Kwiatkowski, 2001; Meyer-Bäse, 2004; Shapiro and Stockman, 2001). The learning sequence is a set of feature vectors x_i and class numbers j, which contains objects described by those features. Therefore, the learning sequence for the j class, which is a sub-set of and S sequence is illustrated by the following formula:

$$S_j = \{x_{j,k} \in X, k = 1, 2, \ldots, N_j\}, \quad j \in M \tag{2.4}$$

The task of the supervised recognition system at the learning stage is to observe the input and output information presented by a trainer, and fitting the recognition algorithm to a problem on the basis of the received response, which is compared to the expected response (Cichosz, 2000). According to the probabilistic approach, the supervised recognition is described as an estimation problem of probability density distribution $P(X|Y)$, where (X, Y) are random variables with a common distribution $P_r(X, Y)$ (Hastie et al., 2001).

As it was mentioned, the recognition algorithm Ψ maps the feature space on a set of class numbers (2.3), which can be represented as generating feature space distribution on decision areas (2.5), that is on a disjoint set family (2.6) and a set family, which covers the entire X feature space (2.7) (Kurzyński, 1997).

$$D_x^i = \{x \in X : \Psi(x) = i\}, \quad i \in M, \tag{2.5}$$

$$D_x^i \cap D_x^j = \oslash, \quad i, j \in M, \quad i \neq j, \tag{2.6}$$

$$\bigcup_{i \in M} D_x^i = X \tag{2.7}$$

Description of decision areas can be conducted on the basis of the so called decision functions (g_i, discriminating function) (2.8), which are selected in such a way that function with index i has greater value in the $i - th$ decision area than in other decision areas (*majorization rule, maximum rule*) (2.9).

$$g_i : X \to R, i \in M \tag{2.8}$$

$$\forall_{i \in M} \vee_{x \in D_x^{(i)}} g_i = \max_{k \in M} g_k(x) \tag{2.9}$$

Description of supervised recognition process is graphically presented as a scheme (Fig. 2.1).

Unsupervised classification
It is possible to talk about an entire group of unsupervised recognition methods and numerous authors give examples of their application in remote sensing and image
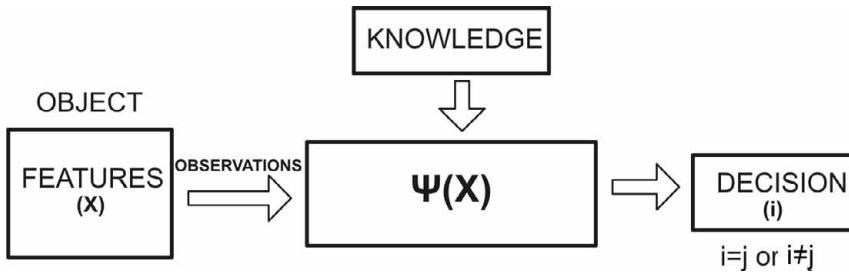
Figure 2.1. Supervised classification scheme

analysis (Aplin and Atkinson, 2001; Atkinson and Lewis, 2000; Chang et al., 2002). Those methods identify clusters of points that represent object features without the training information participation (expert's knowledge), just on the basis of points distribution in the X space. The system, while analyzing the input vector sequence $x^{(i)}$, should be able to determine the correct answers (output variables) (Cichosz, 2000). According to the probabilistic approach, the recognition training system receives a number N of observations $(x_1, x_2, \ldots, x_N)$ concerning the properties of an object (characterized by certain distribution of probability) and its task is to infer about the type and parameters of the distribution without the trainer's aid (Hastie et al., 2001).

Supervised methods offer an easy to accomplish possibility of training quality determinations and recognition via comparison of classification results with the test pattern (verifying sequence that is similar to the training sequence, but not used for training), for example as a loss function $L(i, j)$ which evaluates the loss caused by the classifying an object from class i into a class j. Unfortunately, due to the lack of a pattern in unsupervised classification, this type of direct measure does not exist.

Due to the fact that classes are distinguished without semantics related to the land surface, and that there is no possibility of direct identification of a number of natural classes of land cover (which may be the sum of several separate decision areas), unsupervised classification methods are rarely employed for land use recognition on remote sensing data and photographs (especially the high resolution photographs) (Duda, 2001). Rapid development of new recognition methods, as well as their non-homogeneous character causes that there is not common standard of their systematization. Tadeusiewicz and Flasiński (1991) attempted to classify the recognition methods. Apart from such methods as structural recognition, decision trees or wavelets, a particular attention should be paid (due to their application in the presented paper) to methods based on artificial neural networks and methods based on probabilistic model. All of the modern approaches and methods used in recognition (artificial neural networks), genetic algorithms or fuzzy and hybrid systems have developed during the last dozens of years, mainly due to the growing computational abilities of computers. The modern methods are based

on much earlier statistic and syntactic methods, which are still used and which very often offer results much better than their successors. The older methods are recommended especially in cases when statistic information and indicators which describe the problem are available (Meyer-Bäse, 2004).

2.1.1. Probabilistic approach

According to the probabilistic approach, in order to accomplish the task of recognition (classification), it is necessary to assume that feature vector x and class index j to which the vector belongs, both constitute a realization of a pair of random variables (X, J), where $X \subseteq R^d$ is a continuous variable, while J variable, which accepts values from $M = \{1, 2, \ldots, M\}$ set is of a discrete type. Random variable X has for all the j values a probability distribution function (2.10), which is also called a conditional distribution of class features.

$$f(x/j) = f_j(x), \quad x \in X \tag{2.10}$$

The probability distribution for J variable is as follows:

$$P(J = j) = p_j, \quad j \in M, \tag{2.11}$$

and is called *a priori* probability of belonging to the class (Kurzyński, 1997). The probability is related to a situation in which measurement information about the object under the process of recognition does not exist, and can only be inferred on the basis of particular classes participation in an object generating source. Moreover, it is necessary to assume the existence of a certain non-negative and limited function, which will be referred to as the loss function:

$$0 \le L(i, j) < \infty, \quad i, j \in M. \tag{2.12}$$

The function describes the loss which is caused by classifying j class object to an class i, thus the consequences of misclassification. In certain situations, such as classification of land cover on satellite or airborne images, an incorrect classification of an object (a pixel) from a certain class to a class to which it does not belong does not implicate a loss greater than the classification of that object to yet another class which is also incorrect. Misclassification of objects causes usually similar loss for the classification process in all the classes. Application of the following function:

$$L(i, j) = \begin{cases} 0, i = j \\ 1, i \ne j, \end{cases} \tag{2.13}$$

called a zero-one loss function in such a situation seems to be reasonable.
Therefore, if the x values are the realization of a random variable X, the recognition result indicated by algorithm Ψ is also a realization of a random variable I. It is a discrete variable and assumes the values from a set M:

$$I = \Psi(X) \tag{2.14}$$

It is possible to determine – on the basis of the described conditions – the possibility of occurrence of an event, when a j class object is classified as belonging to an i class (Kurzyński, 1997):

$$q\left(i/j\right) = P\left(I = i/J = j\right) = \int\limits_{D_x^{(i)}} f_j(x)dx, \quad i,j \in M \tag{2.15}$$

It is equivalent to a statement that recognition algorithm Ψ classifies the feature values of the object from j class to a decision area i. Naturally, $q(j/j)$ stands for the correct classification probability.
The probability

$$P_e\left[\Psi\right] = \sum_{j \in M} p_j \sum_{i \in M, i \neq j} q\left(i/j\right) \tag{2.16}$$

is known as the average probability of incorrect classification of algorithm Ψ.
The expected value of the $L(i,j)$ function is known as the average risk of the decision rule Ψ:

$$\mathbf{R}\left[\Psi\right] = \mathsf{E}\left[L(I,J)\right] = \mathsf{E}_{X,J}\left[L(\Psi(x), J)\right] \tag{2.17}$$

Due to the continuous character of variable X and the discrete character of variable J, the risk $\mathbf{R}[\Psi]$ can be expressed as:

$$\mathbf{R}\left[\Psi\right] = \int\limits_{X} \sum_{j \in M} L(i,j)p_j f_j(x)dx =$$
$$\sum_{j \in M} p_j \sum_{i \in M} L(i,j) \int\limits_{D_x^{(i)}} f_j(x)dx = \sum_{j \in M} p_j \sum_{i \in M} L(i,j)q(i/j) \tag{2.18}$$

The unconditional probability density of variable X equals:

$$f(x) = \sum_{j \in M} p_j f_j(x) \tag{2.19}$$

The probability determined on the basis of Bayes' formula:

$$p_j(x) = \frac{p_j f_j(x)}{f(x)} \tag{2.20}$$

is known as the *a posteriori* probability of belonging to a class. It refers to a specific object, the features of which were measured and are known. It determines the degree of object's belonging to class j.
The case in which the probabilities (2.11) and conditional densities (2.10) are known is called the case of a complete probabilistic information. The algorithm Ψ^*, which minimizes the average risk (2.17):

$$\mathbf{R}[\Psi^*] = \min_{\Psi} \mathbf{R}[\Psi] \tag{2.21}$$

is known as the optimum algorithm or the Bayes algorithm, while the risk $R^* = R[\Psi^*]$ is called the Bayes risk. Thus, minimizing of the average risk applying

rule (2.20) we obtain the following equation (Kurzyński, 1997; Tadeusiewicz and Flasiński, 1991; Żurada et al., 1992):

$$\min_{\Psi} \mathbf{R}[\Psi] = \min_{\Psi} \int_X \sum_{j=1}^{M} L\,(i,j)\,p_j f_j(x) dx = \min_{\Psi} \int_X f(x) \sum_{j=1}^{M} L\,(i,j)\,p_j(x) dx \quad (2.22)$$

As the unconditional feature density function (2.10), which constitutes a part of the above equation, does not influence the decision, it can be omitted. Thus we obtain the following equation:

$$\min_{\Psi} \mathbf{R}[\Psi] = \min_{i \in M} \sum_{j=1}^{M} L\,(i,j)\,p_j(x) = \min_{i \in M} \sum_{j=1}^{M} L\,(i,j)\,p_j f_j(x) \quad (2.23)$$

For the zero-one loss function (2.13) one can notice that the risk minimization of making a mistake can be substituted by the maximization of the correct decision probability:

$$\min_{\Psi} \mathbf{R}[\Psi] = \min_{i \in M} \sum_{j=1,j \neq i}^{M} p_j(x) = \min_{i \in M} (1 - p_i(x)) = \max_{j \in M} (p_j(x)) \quad (2.24)$$

Hence follows a simple decision rule Ψ^* of optimal classification:

$$\Psi^*(x) = i \Rightarrow p_i f_i(x) = \max_{k \in M} p_k f_k(x), \quad (2.25)$$

Thus, the recognized object should be included to a class for which the *a posteriori* probability (or the *a priori* probability multiplied and the feature density class distribution function) is greatest. So, it has a highly intuitive justification.

Classification on the basis of multispectral information is not possible directly by application of Bayes algorithm (2.25) in remote sensing, mostly due to the lack of complete probabilistic information. Researchers ((Atkinson and Lewis, 2000), etc.) assume that the spectral features are characterized by a normal multidimensional distribution (Adamczyk and Będkowski, 2005):

$$f_j(x) = \frac{1}{(2\Pi)^{k/2} |E_j|^{1/2}} \exp\left[-0.5\,(x - m_j)^T E_j^{-1}\,(x - m_j)\right], \quad (2.26)$$

where: m_j − average values vector,
         E_j − feature covariance matrix.

Such an assumption may lead to a parameterization of the recognition task. The basis of the parameterization is to select the distribution parameters and determine the *a priori* probability on the basis of the training sample. In practical applications of the method it is necessary to check whether the distribution normality hypothesis is fulfilled at a satisfactory reliability level. The generalized

multidimensional Kolmogorov-Smirnov test can be employed in such situations (Tadeusiewicz and Flasiński, 1991). Due to the fact that normally the verification of the multidimensional distribution is a difficult task, the aforementioned approach is often employed in order to verify the character of a distribution, or the verification of the hypothesis is conducted via the (one dimensional) feature histogram analysis. Although the suggested approach is contradictory to the postulated need of hypothesis verification, and in the light of the presented remarks is an error, it is widely accepted. The *a priori* probability can be approximated by the quotient, which describes the participation of individual classes in the set of all the objects:

$$\widetilde{p}_j = \frac{N_j}{N}, \quad j \in M, \tag{2.27}$$

where: N_j − number of objects from the class j,
                N − number of all the objects.

It is one of the possible approaches to the recognition problem. Definitely, the normal class density distribution assumption is disputable. Moreover, the assumption of x feature continuity is a considerable limitation in remote sensing, mostly due to the discrete character of the observations (limited radiometric detection). In that case, however, there are no differences in the approach and acting rules of the recognition task. Assuming that the X random variable is discretely distributed, it can be presented by the conditional probability:

$$P(X = x_k/J = j) = p(x_k/j), \quad x_k \in X, \quad j \in M, \tag{2.28}$$

while the unconditional distribution can be expressed as:

$$P(X = x_k) = p(x_k) = \sum_{j=M} p_j p(x_k/j). \tag{2.29}$$

Therefore, the incorrect decision probability equals:

$$q(i/j) = \sum_{x_k \in D_x^{(i)}} p(x_k/j) \tag{2.30}$$

Making allowance for the aforementioned changes leads to the following form of Bayes algorithm for the zero-one loss function (2.13):

$$\Psi^*(x_k) = i \Rightarrow p_i p(x_k/i) = \max_{l \in M} p_l p(x_k/l) \tag{2.31}$$

When information concerning the type and parameters of the distribution is lacking, the solution of the task is reduced to the non-parametrical case. Such an approach is universal and possible to apply in all the recognition tasks, but it is more difficult to implement. The problem can be solved in a number of ways by the employment of the training set. Numerous researchers such as: (Devijver and

Kittler, 1982; Duda and Hart, 1973; Bubnicki, 1969; Ripley, 1996) discuss various algorithms, of which special attention should be paid to the following methods: the smallest interval, k-th nearest neighbor, the nearest neighbor. They are frequently employed in remote-sensing systems of decision support.

2.1.2. Artificial neural networks approach

Historical background

The structure and function of the natural nerve cells in the brain was the basis for the formulation of the first formal model of the artificial neuron by McCulloch and Pitts in 1943 (Tadeusiewicz, 1993). In 1949, Hebb discovered that knowledge can be stored by means of artificial neural networks. The theory had been under development for years, but no spectacular implementation of the invention was made until after the great increase in computer powers in the 1980s. This has caused a revival of the artificial neural networks idea and its implementation in a number of practical tasks.

Natural nervous system

The nervous system of living organism is built of nerve cells, known as neurons. Those cells can receive numerous signals (up to 1000) via entries, called dendrites, and emit one signal from a cell via an appendix called an axon. The cells transfer signals between one another by means of chemical and physical processes which takes place in synapses. Synapses serve as an intermediary. As a consequence of their functioning, the signal can be either amplified or quenched, so that, the signals leaving one neuron and reaching another are modified. If the sum of signals reaching a neuron exceeds a certain value, further signals are sent away from the neuron's entrance. Functioning of a number of artificial neurons and neural networks have been formulated and formalized on the basis of the described, simplified nervous model system. The characteristics of them can be found in a number of papers (for instance: (Tadeusiewicz, 1993; Linh, 2004; Żurada et al., 1992; Duda, 2001)).

Artificial neuron model

The formula describing the functioning of a single neuron can be presented as (Rutkowski, 2005):

$$y = f(s) \qquad (2.32)$$

where: $s = \sum_{i=0}^{n} x_i w_i$,
         n − number of inputs to the neuron,
         $x = [x_1, \ldots, x_n]^T$ − input vector,
         $w = [w_0, \ldots, w_n]^T$ − synaptic weight vector,
         y − output value,
         f − neuron activation function .

The operation of a neuron is as follows: input signals $x_0, \ldots, x_n$ are multiplied by the corresponding weights $w_0, \ldots, w_n$. Next, a sum of products is created, and it is subjected to the operation of the activation function:

$$y(t) = f\left(\sum_{i=0}^{n} w_i(t)x_i(t)\right) \tag{2.33}$$

One of the input signals (x_0) can be distinguished and then its value is constant and equals 1. Its weights w_0 is called bias and constitutes the boundary value of the neuron output activation. The activation function is usually a non-linear function, for instance sigmoidal:

$$f(x) = \frac{1}{1 + e^{-\beta x}} \tag{2.34}$$

Depending on the type of the activation function, the training method (weight modification), and the possible introduction of a feedback, various neurons models can be distinguished.
Given a certain expected neuron response, the error Q of its functioning can be calculated:

$$Q(w) = \frac{1}{2\left[d - f\left(\sum_{i=0}^{n} w_i x_i\right)\right]^2} \tag{2.35}$$

The essence of neuron training consists in finding such a system of weights w_i that the error Q becomes minimal.

Neural networks

The application of a single neuron is rather limited. It is able to divide the n-dimensional input value space into two sub-spaces by means of an (n-1) − dimensional hiperplane (Rutkowski, 2005). More complex tasks can be solved only by neural networks, that is neurons which are specially connected to one another and which are distributed in two or more layers. a number of neuron connection variants exist. The presented paper elaborates on uni-directional networks with a sigmoidal activation function. As the networks are of a lamellar structure and the response error is known only for the output layer, training of such structures is more complicated than in the case of a single neuron. A number of training algorithms related to neural networks can be found in the literature. The method of standard back-propagation based on the maximum fall rule, is

the most widespread method (Rutkowski, 2005). The *Rprop* method is another example of training methods. In most of the tasks, it accelerates the training when compared to the standard back-propagation method, and it is more resistant to the occurrence of error function local minima. The formal training description of neural networks can be found in professional literature (e.g. Tadeusiewicz (1993); Linh (2004); Żurada et al. (1992); Duda (2001)) and is beyond the scope of the presented paper.

When a neural network is presented as a black box (Fig. 2.2), the analogy to the supervised classification system (illustrated on Fig. 2.2) can be observed. Therefore, the classification is one of the key tasks, the solution of which can be reached via the application of artificial neural networks.

Figure 2.2. Neural network as a black box

Examples of artificial neural networks application for classifying land cover using remote-sensing data

Literature concerning information technology and automatics gives numerous examples of neural networks application in various tasks. Among them, an important role is played by studies on the application of neural networks in image processing, where the problem of classification and recognition is crucial. For instance, Miller and her team (Miller et al., 1995)) conducted research on the usability of one-directional neural networks in classification of the content of satellite images. She observed the need to strengthen the feature vector by adding contextual information. She also noticed the need to conduct research on the hidden network layers, which influence the results quality. The studies on the neural network optimal architecture selection and weight initialization in classification task of the multispectral satellite images were conducted by German and Gahegan (1996). They tested various network architectures in order to determine the best one. The researchers compared the results with the approach which was used in relation to the task of conditioning the hidden layer size on the neuron number in the input and output layers.

A number of neural networks applications are also presented in the geodesy and cartography literature. Gil (2006) published an extensive paper on the application of neural networks in geodesy. He touches upon various problems related to engineering and satellite geodesy, which can be solved on the basis of the presented method. Gil offers an interesting connection of *k-means* unsupervised classification

with his own distance minimization algorithm of the Kohonen's neural network weight vector, trained by means of the Winner Takes All (WTA) competitive method. In the author's opinion, the developed classifier set allows to achieve results better than any of the methods used separately, and the set can be successfully employed to the studies of issues related to remote-sensing data classification. A number of experiments employing the neural networks used as satellite and air image content classifiers have been described by Iwaniak, Paluszyński, Kubik and Tymków (Kubik et al., 2004, 2005, 2006a,b; Iwaniak et al., 2005, 2006). The results presented in the aforementioned publications prove the efficacy of a classification based on artificial neural networks used for the purpose of land cover classification on satellite imagess. In most of the studies, the images from Landsat TM were used. CORINE land cover map was used as the classification pattern. The classification results were evaluated as very good, and their comparison to the manual classification showed agreement at the middle level of the $\hat{\kappa}$ coefficient (which exceeded 0.9). The results of studies conducted by other authors who focused on using a similar air image content classification were unsatisfactory. An attempt at an automatic recognition of classes of buildings on color, high resolution photogrammetric pictures – done exclusively on the basis of the RGB pixel value and by means of neural network construction with allowance for contextual information of a classified pixel – was satisfactory. However, application of the same method for asphalt roads recognition may be considered unsuccessful.

2.2. Data sources for the automatic supervised land cover analysis

A number of measuring techniques can be applied in the process of land cover class identification used for estimation of the resistance coefficients. Particular attention should be paid to: airborne and terrestrial laser scanning, and both airborne and satellite imagery.

2.2.1. Airborne laser scanning as the source of data for digital terrain model and digital surface model generation, as well as information concerning the forest floor

Airborne laser scanning is an advanced data acquisition technology which comprises three modern measuring techniques: GPS (Global Positioning System), INS (Inertial Navigation System) and LRF (Laser Rangefinder). The cooperation scheme of the three techniques is illustrated in Fig. 2.3.

Airborne laser scanning – principle of operation
A laser device, which is installed on the aircraft, sends impulses at various angles, usually perpendicularly to the direction of the aircraft flight. On the basis of the measurement of signal running from the transmitter to the measured object (point)

and its return to the receiver, the distance between the aircraft and the ground
surface (or the object which caused the reflection of the signal) is measured.

Spatial position of an aircraft is determined by GPS in the Differential Ground
Positioning System (DGPS) mode. It means that an antenna and a GPS receiver
have to be placed on the aircraft and on at least one permanent point on the ground
surface. INS determines the orientation of the aircraft in relation to the external
system by the measurement of three angles: pitch, roll and yaw. The entire system
determines the positioning of points in spatial the coordinate system in which the
angle and distance from points are measured by means of a laser scanner. GPS
determines – in one second time intervals – the positioning of the polar system
point of origin, while INS determines its constantly changing orientation. Accurate
processing of the data coming from the three systems gives the points coordinates
in the WGS84 cartesian coordinate system. Knowledge of the ground-based point
coordinates on which the GPS antenna is placed, as well as the knowledge of
the geoid's altitude on the studied area, enables to determine coordinates in the
coordinate system and the altitude system used in a given area (Borkowski et al.,
2006a).
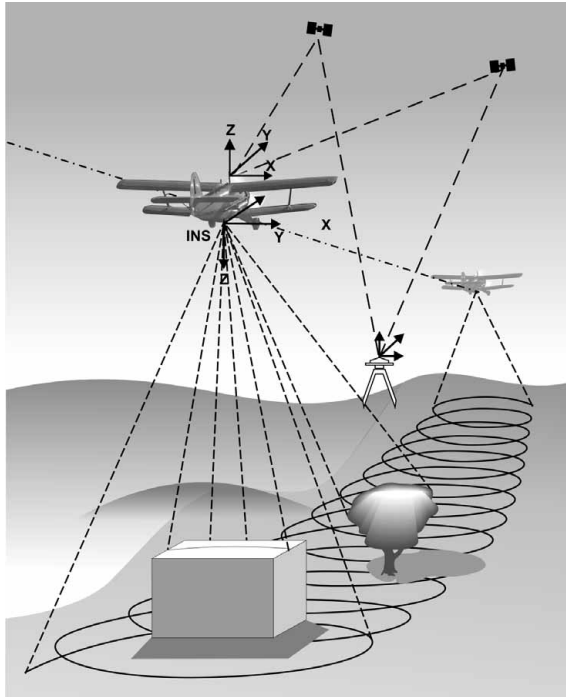
Figure 2.3. Airborne laser scanning components (Borkowski, 2006)

2.2.2. Terrestrial laser scanning as the source of plant parameters

The principle of operation of terrestrial laser scanning is similar to the one present in airborne laser scanning. Here, the system is also composed of a transmitter, that is a device which produces the laser beam (emission of a coherent light beam is its main feature), and a receiver, which is a device that collects the returning data beam. There is no need, however, to register the device position during the measurement (lack of INS), as it is placed on a tripod and is immovable. It is necessary to determine the coordinates of measurement points and of calibration points.

Application of the terrestrial laser scanning for the purposes of making inventories in forests has been the subject of intensive development works during the last few years (Aschoff et al., 2004; Chasmer et al., 2004; Barilotti et al., 2006; Buddenbaum and Seeling, 2006; Ducic et al., 2006; Koch et al., 2006; Straub et al., 2006; Lucas et al., 2006). It is possible to determine the forest stand affluence, average tree heights and diameters at breast height, as well as the distribution of trees on the basis of terrestrial laser scanning. Knowledge of the aforementioned parameters is also essential for the correct evaluation of hydraulic characteristics of the area, which became the inspiration for employing the described technology in the field of flood-plain hydraulics. Studies on the application of terrestrial laser scanning technology were conducted lately by Warmink, Middelkoop and Straatsma from the University of Utrecht (Warmink et al., 2006). They managed to describe an experiment aiming at the measurement of the *Vegetation Area Index* and determination of *vegetation density* on the Lower Rhine floodplain in Holland. The researchers' results were confronted with direct measurements and were evaluated as satisfactory. They managed to prove that the conventional measuring methods can be successfully replaced by scanning. However, in case of areas densely covered by shrubs and saplings, the accuracy and effectiveness of measurement decreases considerably. Nevertheless, terrestrial scanner serves as a very useful device when employed to making forest inventories. **Therefore, application of the scanner in the inventory of training samples for the flood-plains' supervised classification – as a response to the hydraulic modeling needs – should also be taken into consideration.**

2.2.3. Air photographs and satellite images as the sources of data on spectral reflection and texture

Diversified reflection (and sometimes also emission) of the electromagnetic radiation by various field objects, and image registration in various spectral ranges allow conducting an automatic classification and analysis of image content. Satellite images are most often used for that purpose. Registration of a number of spectral channels allows determination of various classes of objects characteristics. Classification in multidimensional spectral response space or analysis of colored compositions give satisfactory effects in of numerous environmental issues. Spatial resolution of such imageries is usually at the level of a dozen to hundreds meters

(e.g. Landsat TM – circa 30 meters for most of the channels). When high resolution images are employed (e.g. Ikonos), the detail, and therefore diversification of content, make the classification process more difficult.

Classical photogrammetric images cannot be easily automatically classified, due to the lack of multispectral image registration. In the case of colored pictures, the feature vector can be based on color space channel values (e.g. RGB or HSV); the received information, however, is poor in comparison to multispectral imagery. Texture feature values of the registered areas may serve as another classification support. Nevertheless, results of automatic air photographs classification are definitely inferior to manual vectorization and are not commonly employed for map creation in the nearest future.

Air images are widely used in forestry. However, forest analysis usually requires image registration on the material or by means of sensors which are sensitive not only to the visible but also to the infrared light.

2.3. Evaluation of the classification quality

Evaluation of the supervised classification quality for the training data does not pose any problems. However, it does not deliver reliable information on the results quality. Verification of the recognition quality is conducted on a prepared test data set, that is a vector set and the expected response of a classifier that were not been used previously in the training process. The process is illustrated in Fig. 2.4.
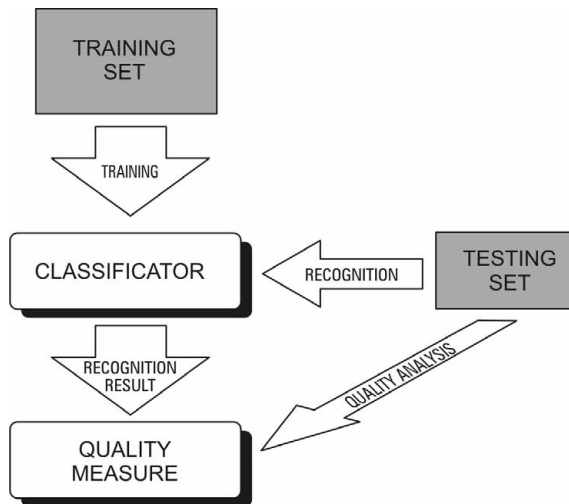
Figure 2.4. Recognition process joined with quality analysis

Various measures can be applied to the quantitative description of classification quality. Researchers (e.g. Adamczyk and Będkowski (2005)) postulate that the *error matrix* $A = [a_{ij}]$ methods should be employed. The matrix determines a number of points belonging to class j, which were classified as points belonging to class i. The error matrix structure can be presented as follows (Kubik et al., 2006b):

Belongs to a class		According to the standard			
		1	2	...	M
According to the classifier	1	a_{11}	a_{12}	...	a_{1M}
	2	a_{21}	a_{22}	...	a_{2M}
	...	...	...	...	...
	M	a_{M1}	a_{M2}	...	a_{MM}

In the case of the classification results evaluation for only one class, the table can be presented as follows:

Belongs to a class		According to the standard	
		yes	no
According to the classifier	yes	a_{11}	a_{12}
	no	a_{21}	a_{22}

A number of parameters can be calculated on the basis of the defined error matrix (Foody, 1960; Hubert-Moy et al., 2001; Adamczyk and Będkowski, 2005; Kubik et al., 2006b):

— share of correctly classified pixels I_{cp} – the sum of correctly classified pixels to the total number of pixels under consideration:

$$I_{cp} = \frac{\sum_{t=1}^{M} a_{tp}}{a}, \tag{2.36}$$

— user accuracy of class i:

$$u_i = \frac{a_{ii}}{a_{ri}}, \tag{2.37}$$

where: $a_{ri} = \sum_i a_{i.}$ (sum of elements in i line);
— producer accuracy of the class i:

$$p_i = \frac{a_{ii}}{a_{ci}}, \tag{2.38}$$

where: $a_{ci} = \sum_{ij} a_{i.}$ (sum of elements in i column);
— total accuracy d of classification:

$$d = \frac{\sum_i a_{ii}}{a_t}, \tag{2.39}$$

where: $a_t = \sum_i a_{ci} = \sum_i a_{ri}$ (total number of points);

— simple Kappa coefficient:

$$\hat{\kappa} = \frac{P_o - P_e}{1 - P_e} \ , \ \ \text{where} \ \ P_o = \frac{\sum_i a_{ii}}{a_t} \ \ \text{and} \ \ P_e = \frac{\sum_i a_{ri} a_{ci}}{a_t^2} \tag{2.40}$$

— weighted Kappa coefficient:

$$\hat{\kappa}_w = \frac{P_{o(w)} - P_{e(w)}}{1 - P_{e(w)}}, \quad \text{where} \ \ P_{o(w)} = \frac{1}{a_t} \sum_i \sum_j w_{ij} a_{ij} \\ \text{and} \ \ P_{e(w)} = \frac{1}{a_t^2} \sum_i \sum_j w_{ij} a_{ri} a_{cj} \tag{2.41}$$

Weights w_{ij} should fulfill the following condition: $0 <= w_{ij} < 1$. Weight of each class can be calculated on the basis of its size.
Fleiss (1981) offered the following interpretation of the weighted coefficient:

$$\kappa > 0.75 \qquad \text{substantial agreement}$$
$$0.4 < \kappa \le 0.75 \qquad \text{moderate agreement}$$
$$\kappa \le 0.4 \qquad \text{poor agreement of the compared images.}$$

Landis and Koch (1977) offer a different interpretation of agreement:

$$0.81 \le \kappa \le 1 \qquad \text{almost perfect agreement}$$
$$0.61 \le \kappa \le 0.80 \qquad \text{substantial agreement}$$
$$0.41 \le \kappa \le 0.60 \qquad \text{moderate agreement}$$
$$0.21 \le \kappa \le 0.40 \qquad \text{fair agreement}$$
$$0.00 \le \kappa \le 0.20 \qquad \text{slight agreement}$$
$$\kappa < 0.0 \qquad \text{poor agreement}$$

Chapter 3

Automatic floodplains valorization with respect to flow resistance as exemplified by a stretch of the Widawa river valley

3.1. Description of the study area

Widawa is a right-bank tributary of the Odra river, joining Odra at its 266.9 kilometer at the altitude of 110 metres above the see level. The length of Widawa, which originates in Twardogóra Hills at the altitude of 204 metres above see level, is approx. 103 km. Its watershed is estimated at 1716.1 km^2. Widawa is a lowland river and on the major part of its length, it is situated in a gently sloping, wide and flat river valley. Due to its shallow bed, Widawa often floods the surrounding areas. The river segment under examination is partly embanked and controlled. It flows through developed areas, and at its estuary it flows through agricultural areas and forests. The studied area covered approx. 10 kilometres of the final stretch of the river, to its estuary in the Wrocław administrative area. This area was chosen for investigation due to its good recognition with respect to its hydraulics and diversified land cover.

3.2. Site survey

The following elements of site survey were conducted in order to prepare a numerical terrain model and its classification with respect to flow resistance:

— Airborne laser scanning,
— Preparation of non-metrical air photographs,
— Land survey aiming at making an inventory of the land-cover classes inventory, supplemented by a terrain laser scanning.

3.2.1. Airborne laser scanning

A prototype *ScaLars II* scanner was used in the project (it was constructed in the Navigation Institute of Stuttgart University). The scanner uses a continuous wave (CW) and its beam is deflected by means of a rotating mirror. Assembly of the mirror rotation and the airplane movement results in the survey points distribution along the ellipsis moving on the scaned area. The system records also the intensity of the beam reflection. The most important parameters characterizing

the scanner are presented in Tab. 3.1. The Applanix system was employed to register the GPS and INS signal.

Table 3.1. *ScaLars* system parameters (Borkowski et al., 2006b)

Laser power	0,8 W
Wave length	810 nm
Footprint diameter	5 cm
Measurement frequency (CW)	1 MHz, 10 MHz
Measurement range	750 m
Measurement accuracy (H=700 m)	0,12 m
Beam deflection method	Rotating mirror
Beam deflection from the flight direction	7,60
Beam deflection from direction perpendicular to flight direction	13,60

Registration of the GPS signal was possible due to the application of Trimble 4700 receivers. The scanned area width equaled circa 2 kilometers. The project parameters during the airborne scanning were the following:

— Flight speed: 150 km/h,
— Altitude: 550 m,
— Scanned belt width: 280 m,
— Space between flight axes: 190 m.

Two to three points per square meter were registered on average. The average distance between the neighboring points on individual scans is about 0.6 m. A digital terrain model and a digital surface model were constructed in the Geodesy and Geoinformatics Institute of the Wrocław University of Environmental and Life Sciences on the basis of the collected points (x, y, z) information. A flakes method was employed in order to recognize the points which were not reflected by the surface (Borkowski, 2005). The models were constructed on the basis of fragments related to the classification areas presented in 3.3.1 subchapter. Subtraction of complementary model area points and model land-cover points resulted in the information concerning the height of land-cover forms, which was used later in the supervised classification process (Tymków and Borkowski, 2006; Tymków et al., 2006). Moreover, the point data were used to estimate the vegetation density on various levels above the land surface (subchapter 3.3.3).

3.2.2. Aerial photographs

In order to acquire image information about the studied area within a couple of days from the airborne laser scanning, circa 200 non-metrical air photographs were taken by means of Nikon d70s digital camera (resolution; 5 million pixels). 70% of the studied area was covered by the photographs. The altitude from which the photographs were taken was circa 800 m above see level. An example of
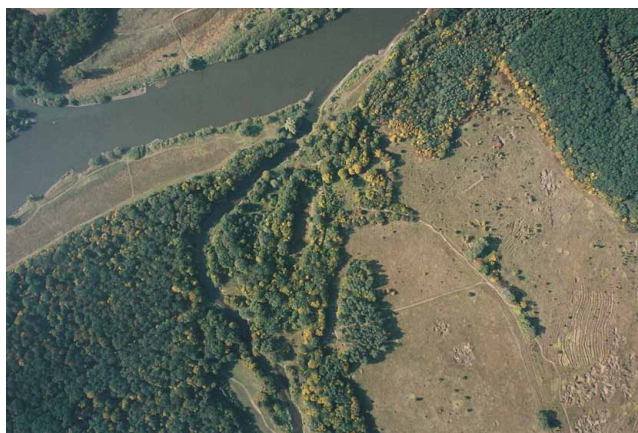
Figure 3.1. Non-metrical air photograph presenting the estuary part of the Widawa river taken from a Wilga airplane

a photograph (before picture calibration and photomapping) is presented as in Fig. 3.1.

3.2.3. Determination of the land cover of training sites and verification areas

During the site survey, inventory of the studied area land cover was conducted. It allowed to distinguish 17 land cover classes, 6 of which belonged to tall plants (trees). Two test fields, 50 x 50 m each, were chosen for each class and characteristics of tall plants were analyzed and measured. Moreover, average height, diameter at breast height and distribution of trees growing in forests were measured. The measuring sample equaled 10 trees per each test field. Moreover, location of the two fields was established via GPS and photographs illustrating both fields were taken. Average geometric parameter values of plants and the estimated resistance coefficient for each class (either calculated or copied from Ven Te Chow's tables) are presented in Tab. 3.2.

Table 3.2. Identification of the surface roughness classes of the study area and determination of their parameters

Class number	Description	Image
	Tall plants	
1	Dominating species: populous, height: 30 m. Average plant spacing: $a_x = a_y = 6,3$ m. Average diameter: $0,45$ m. Numerous saplings and shrubs present in the undergrowth. Surface roughness coefficient λ_p calculated on the basis of the 1.10 formula for the assumed water surface level under the branch level ($h = 1.5$ m): 0.366	
2	Dominating species: oak. Height: 10.2 m. Average plant spacing: $a_x = a_y = 0.85$ m. Average diameter: $0,09$ m. Sparse undergrowth. Surface roughness coefficient λ_p calculated on the basis of formula 1.10 for the assumed water level below the branch level ($h = 1.5$ m): 0.779.	
3	Dominating species: oak, elm. Height: 15.4 m. Average plant spacing: $a_x = a_y = 0.90$ m. Average diameter: $0,50$ m. Numerous saplings and shrubs in the undergrowth. Surface roughness coefficient λ_p calculated on the basis of formula 1.10 for the assumed water level below the branch level ($h = 1.5$ m): 1.433.	

Class number	Description	Image
4	Dominating species: oak. Height: $18,2$ m. Average plant spacing: $a_x = a_y = 1.2$ m. Average diameter: $0,19$ m. Surface roughness coefficient λ_p calculated on the basis of formula 1.10 for the assumed water level below the branch level ($h = 1.5$ m): 0.993.	
5	Dominating species: willow, oak, elm. Height: $16,4$ m. Average plant spacing: $a_x = a_y = 2,8$ m. Average diameter: $0,27$ m. Numerous saplings and shrubs present in the undergrowth. Surface roughness coefficient λ_p calculated on the basis of formula 1.10 for the assumed water level below the branch level ($h = 1.5$ m): 0.208.	
6	Dominating species: oak. Height: 27 m. Average plant spacing: $a_x = a_y = 18,4$ m. Average diameter: $1,10$ m. Surface roughness coefficient λ_p calculated on the basis of formula 1.10 for the assumed water level below the branch level ($h = 1.5$ m): 0.107	

Class number	Description	Image
Low plants and arable lands		
7	Meadow, roughness coefficient n, according to (Chow, 1959): min. 0.030, average 0.035, maximum 0.050	
8	Meadow with single shrubs, roughness coefficient n, according to (Chow, 1959): min. 0.035, average 0.050, maximum 0.070	
9	Stubble field, roughness coefficient n, according to (Chow, 1959): min. 0.020, average 0.030, maximum 0.040	
10	Ploughed land, roughness coefficient n, according to (Chow, 1959): min. 0.020, average 0.030, maximum 0.040	

Class number	Description	Image
11	Sprouting crops, roughness coefficient n, according to (Chow, 1959): min. 0.030, average 0.040, maximum 0.050	
12	Polders – the floodplain, meadows vegetation, roughness coefficient n, according to (Chow, 1959): min. 0.030, average 0.035, maximum 0.050	
Waters		
13	Running water – river-bed proper. Surface roughness coefficient n for a selected river-bed of the Widawa river type, according to (Chow, 1959): minimum 0.045, average 0.050, maximum 0.060.	
14	Stagnant water. Determination of the roughness coefficient requires determination of the bottom material on the basis of site inspection. For example, roughness coefficient n for earth reservoirs equals, according to (Chow, 1959): minimum 0.025, average 0.027, maximum 0.033.	

Class number	Description	Image
	Urban areas	
15	Buildings − they are treated as local obstacles	
16	Asphalt roads, roughness coefficient n, according to (Chow, 1959): minimum: 0.017, average: 0.020, maximum 0.025	
17	Railroads − when situated along the river flow − the resistance coefficient n, according to (Chow, 1959): minimum 0.020, average 0.030, maximum 0.035. When situated perpendicular to the river flow, they are treated as a wide top overfall.	

3.3. Data integration

3.3.1. Calibration and photomapping of aerial images

Non-metric aerial images taken as a part of site surveys are burdened with gross geometric errors. For geometric correction, they were registered in the coordinate system PUWG 1992 via projective transformation with the use of the nearest neighbor resampling method. In case of areas without details on the map (such as meadows), pictures were adjusted to topographic map with the use of reference points acquired by digitization and some specific identifiable points measured in the field. Ten adjustment points were used on average for a single picture. The accuracy of adjustment was circa 3–4 meters and was accepted adequate. Due to the amateur method of picture acquisition, gross adjustment errors occurred. However, this does not have a negative effect on methodology of image classification. The standard tonal adjustment method was applied during the process of
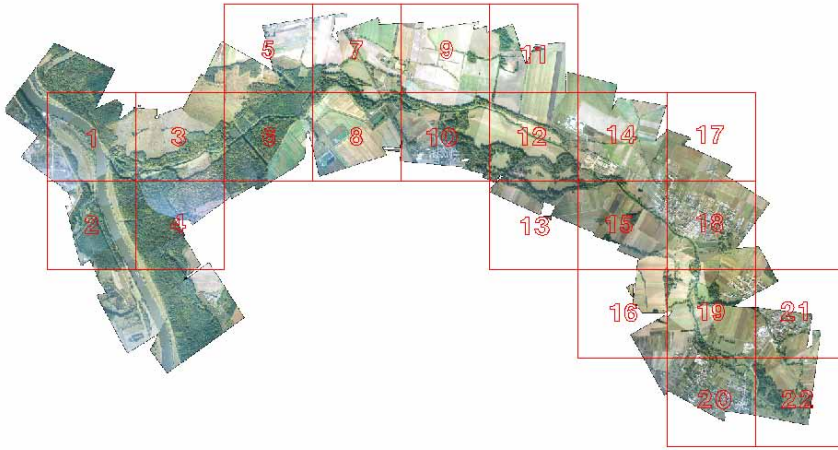
Figure 3.2. Mosaic of aerial pictures for the study area with marked division of computational sections

photomapping. Spatial resolution of pixel was 1 meter. Fig. 3.2 shows the result of photomapping.

On account of computational complexity of the process of recognition, the mosaic was divided into squares of 1000x1000 m spatial dimension in accordance with the grid on the topographical map, which constituted the data for classification.

3.3.2. Height estimation of land cover forms

Using a hierarchic method of points filtering situated outside the land surface, digital terrain model (DTM) and digital surface model (DSM) were constructed on the basis of airborne laser scanning. The flakes-based filtering method was adopted when constructing these models (Borkowski, 2005). They were constructed in stages, with 1 m resolution, creating 1x1 km fragments (like in the case of aerial pictures). Height accuracy determination of the models was estimated to be below 0.5 m. Fig. 3.3 and 3.4 show colourful visualization of the terrain model and the surface model.

By subtraction the altitude coordinates values of the digital surface model from altitude coordinates of the digital terrain model a height model (DM) of land cover forms was obtained. Data were transformed into 8-bit space of shades of grey (Fig. 3.5) and were included in the feature vector of recognizable cover grades.

3.3.3. Estimation of forest floor data

Raw scanning data contain a series of survey points which are reflections from various forms of land cover. In forest areas a part of the registered points represents
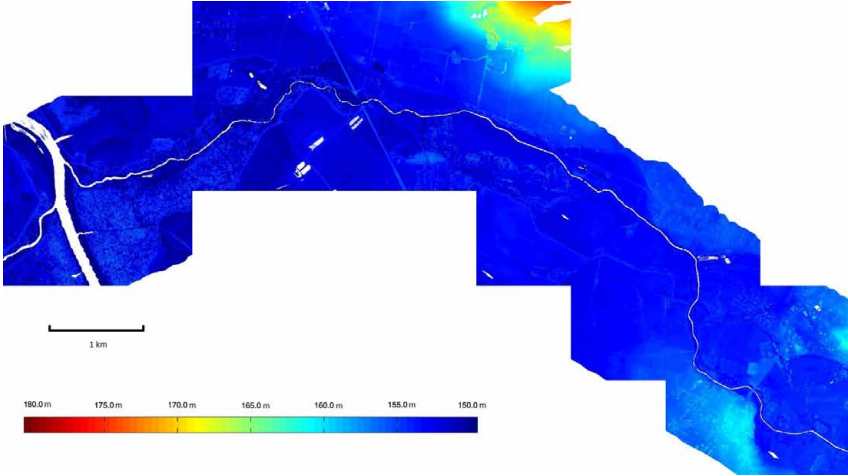
Figure 3.3. Colour visualization of the digital terrain model of the study area
(author: G. Jóźków)
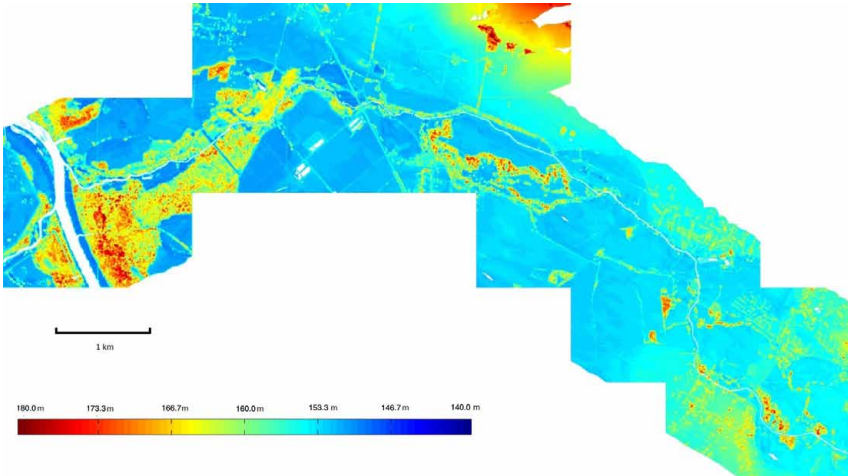
Figure 3.4. Colour visualization of the digital surface model of the study area
(author: G. Jóźków)
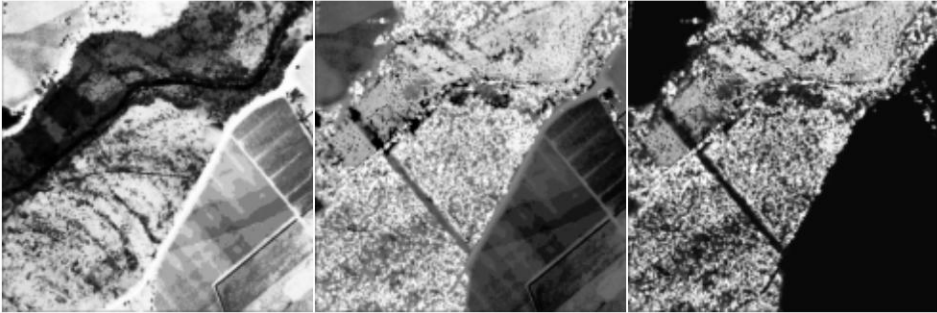
Figure 3.5. Visualization of elevations obtained from laser scanning (from left):
DTM, DSM, DM
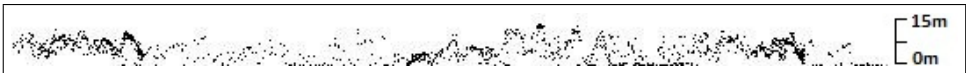
Figure 3.6. Fragment of a vertical section of survey points in a woodland area

reflections from land surface and the other part reflections from vegetation on
different levels. Due to the fact that laser rays have the ability to penetrate forest
areas, a change in tree density can be estimated on the basis of the number of
laser ray reflections (a number of points) at separate levels above land surface.
Fig. 3.6 presents a fragment of a vertical section through measured data. It was
obtained from the cloud of recorded points by cutting it with 1 m distant planes.
If at least one recorded reflection in one section, a plant was assigned (1 m grid).
Then, on the basis of the previously derived digital terrain model, the planes were
transformed into surfaces which were parallel to the land surface. Thus, binary
information about the occurrence of reflection on the specific height above the
land surface was obtained. Fig. 3.6 shows section of projection onto a vertical
plane of 1 m − wide land strip (that correspond to 1 pixel). In the section there
are reflections of land surface line and, above it, reflections from the canopy and
a forest floor line. In some places, an obvious gap between the canopy line and
the land can be seen. On the basis of this profile the average height of the first
level of branches above the land surface can be determined and it is possible to
conclude that thick vegetation occurs in the forest floor.

Information about the occurrence of reflections on specific levels constitutes
1 m special resolution model (named in this work as LEV) which may be shown
graphically in the form of binary images. In total 30 sections spaced at 1 m were
obtained (the highest canopy height was about 30 m). Fig. 3.7 presents three
examples of sections at the levels: 2, 10 and 20 metres above the land surface.
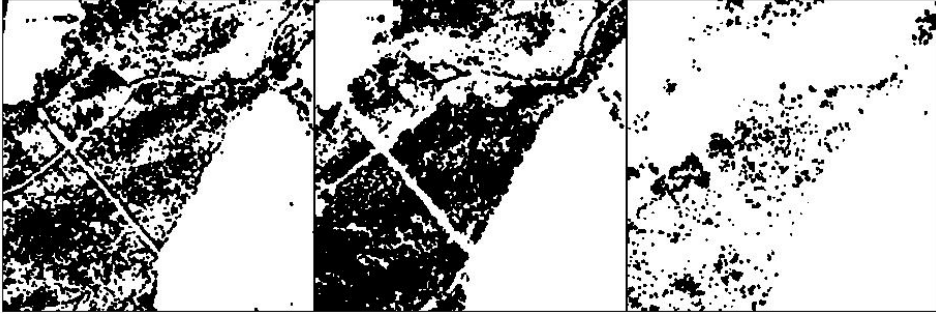
Figure 3.7. Fragment of visualization of information about the recorder reflections at specific levels above the land surface. From left: 2 m level, 10 m level, 20 m level

3.3.4. Image texture analysis

Texture constitutes a very important feature of images. It enables to carry out segmentation or supports the process of recognition in the macroscopic scale. The method of extraction of texture features applied in this research belongs to a whole range of methods which use proximity of pixels in the analyzed image. This method involves constructing a matrix which characterizes the frequency of pixels of specific value in proximity to the others in specific direction in the whole image or in its fragment only.

The adjacency matrix is described with the use of distances and angles (parameters of the analysis). Distance equal 1 indicates a direct pixels proximity, whereas the angle indicates a specific pixel in the analyzed proximity. Specific numbers in the adjacency matrix mean neighbouring frequency of one shade pixel to the other shade pixel. The GLCM (*Grey Level Co-occurrence Matrix*) adjacency matrix can be defined as follows:

$$V_{l,\alpha}(i,j) = |\{((r,s),(t,v)) : I(r,s) = i, I(t,v) = j\}| \qquad (3.1)$$

where: $i, j = 0, \ldots, N-1$ gray levels of points on the picture situated
at the distance of l in the α direction,
N − number of gray levels,
$I(x,y)$ − pixel value of (x,y) coordinates,
$(t,v) = (r + l\cos\alpha, s + l\sin\alpha)$.

The adjacency matrix V is a square matrix and its size is determined by the amount of gray levels of an image. The columns of GLCM matrix represent grey levels of neighbouring points, whereas rows − gray levels of reference points.

The matrix is subjected to symmetrization and normalization in the course of calculations. The symmetry is obtained by adding the matrix and its transposition and, then, by dividing it by 2:

$$\bar{V}_{l,\alpha} = \frac{V_{l,\alpha} + V_{l,\alpha}^T}{2} \tag{3.2}$$

Normalization consists in reducing the values in the matrix to the $\langle 0, 1 \rangle$ interval, according to the formula:

$$P_{i,j} = \frac{\bar{V}_{l,\alpha}(i,j)}{\sum\limits_{i,j=0}^{N-1} \bar{V}_{l,\alpha}(i,j)} \tag{3.3}$$

Only a symmetric and normalized GLCM matrix can determine statistical features of the analyzed land. The symmetry enables analyzing only pixels at one of the angles in a specific direction, in other words, GLCM matrixes are similar at 90º and 270º. Calculations for different angles and distances are analyzed separately or averaged. The following parameters, obtained on the basis of GLCM matrix analysis, were used in this project:

— contrast

$$\sum_{i,j=0}^{N-1} P_{i,j}(i-j)^2 \tag{3.4}$$

— dissimilarity

$$\sum_{i,j=0}^{N-1} P_{i,j}\,|i-j| \tag{3.5}$$

— similarity

$$\sum_{i,j=0}^{N-1} \frac{P_{i,j}}{1+(i-j)^2} \tag{3.6}$$

— maximum $P_{i,j}$ in a mask

$$\max(P_{i,j}) \tag{3.7}$$

— ASM (Angular Second Moment)

$$\sum_{i,j=0}^{N-1} P_{i,j}^2 \tag{3.8}$$

— energy

$$\sqrt{ASM} \tag{3.9}$$

— entropy

$$\sum_{i,j=0}^{N-1} P_{i,j}(-\ln P_{i,j}) \tag{3.10}$$

The method which enables to calibrate the number of shades of grey to the range $0 \div 255$ was implemented. Due to the computational complexity, reduction in the shade number is recommended. The cover classification quality of aerial images is influenced by GLCM mask window which depends on the qualified objects type and the image scale. To achieve satisfactory results, an optimal mask size for specific phenomena and scales need to be determined. Interpretation of the obtained GLCM parameters may be simplified by presenting these parameters in a graphic form by linear transformation into an 8 bit space.

The results of the GLCM method contain seven basic parameters described above which constitute average features for every neighbouring direction. In addition, it is possible to use these features in the same form for each of the separate directions, without averaging.

3.3.5. Beam reflection intensity of airborne laser scanning

Airborne laser scanning provides not only geometric information in the form of coordinate points, but also data about intensity of laser beam reflection. The intensity value depends basically on the type of land cover (it strongly depends on moisture) and, moreover, it may be a valuable source of information in the classification process. The scanning laser emits its own radiation. Assuming that the reflecting surface is homogeneous, the reflected radiation intensity I is proportional to the pulse power P and the reflection coefficient of the puls-illuminated surface, and inversely proportional to the square of the distance between the sensor and the topographical surface h (Mikrut et al., 2006):

$$I \approx \frac{P \cdot r}{h^2} \tag{3.11}$$

The coefficients for specific land cover forms are show in Tab. 3.3 (Mikrut et al., 2006).

Table 3.3. Reflection intensity values of different land cover forms

Surface type	Reflection coefficient (%)
Snow	$\sim 80 - 90$
Deciduous forest	~ 60
Sand	$\sim 50 - 40$
Coniferous forest	~ 30
Buildings (different roofing)	$\sim 20 - 30$

The laser ray is absorbed by water and dark surfaces (e.g. asphalt roads). The intensity image may be helpful to determine precisely the course of a real river bed when it is covered by tree canopies, as well as in locating stagnant water reservoirs (which often have diversified colours), and in improving roads and building recognition. Fig. 3.8 presents exemplary image of reflection intensity in a palette

of colours. Waters are distinctly visible and it is possible to locate forest areas and flood embankments.

Katzenbeisser (2003) examined the usefulness of reflection intensity in the forest area analysis. The analysis carried out by Katzenbeisser contains a detailed description of specific laser pulse registration in vegetated areas. He applied an instrument which allowed to register many reflections of just one pulse. This feature made Katzenbeisser's instrument different from the instrument applied in this project, which used continuous wave in measurements. It examined, for example, the reduction of intensity of a single beam reflected from a forest area. According to Katzenbeisser' analysis, reflection intensity data is difficult and complicated to use. Intensity constitutes a reliable piece of information about surveyed land but only in the case of flat surfaces. In forest areas, where partial reflection from successive vegetation levels occurs, many additional parameters should be taken into consideration in the intensity analysis.

Song, Han and Kim (Song et al., 2002) conducted research on classes of land use using reflection intensity data. The results they obtained for classification of vegetated areas were not satisfactory. The reason for this is the fact that the intensity value of different vegetation types (e.g. grass and trees) is similar and equals about 50%. However, in conclusions, it was stated that the classification quality could be significantly improved by using elevation data from airborne laser scanning.

Charaniya, Manduchi and Lodha (Charaniya et al., 2004) conducted research on features related to laser measurement, such as: normalized height, which is the difference between DTM and DSM; texture which is determined on the basis of local height change, the difference in height between the first and the last pulse and reflection intensity. They used these pieces of information to delineate forest areas with the use of parametric supervised classification which employs Gauss' model and *Expectation-Maximization (EM)* algorithm. They achieved good results. Moreover, they observed that classification may be improved by using airborne images as the source of additional data. Independently, the author of the present work developed a similar idea of feature vector construction for supervised classification in order to assess land cover forms which are homogeneous in terms of flow resistance. This idea has been presented in a number of publications (Mokwa and Tymków, 2004; Tymków and Mokwa, 2005; Tymków et al., 2006).

3.4. Supervised classification of a stretch of the Widawa valley and analysis of the results

In the process of the supervised classification the first stage constitutes preparation of two data – called the teaching one (in other words a pattern) and the test one. The set of teaching vectors must be selected in a way to be representative for a problem and to characterize it effectively. The teaching set must consist not only of input vectors, but also of the output vectors which are the expected respond
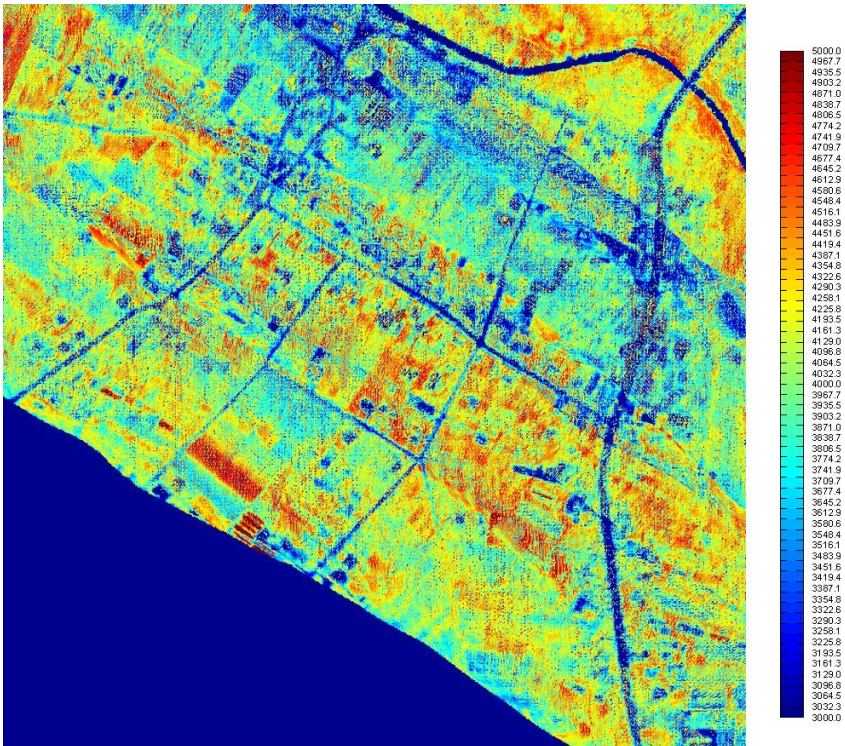
Figure 3.8. An exemplary image of reflection intensity in a colour palette
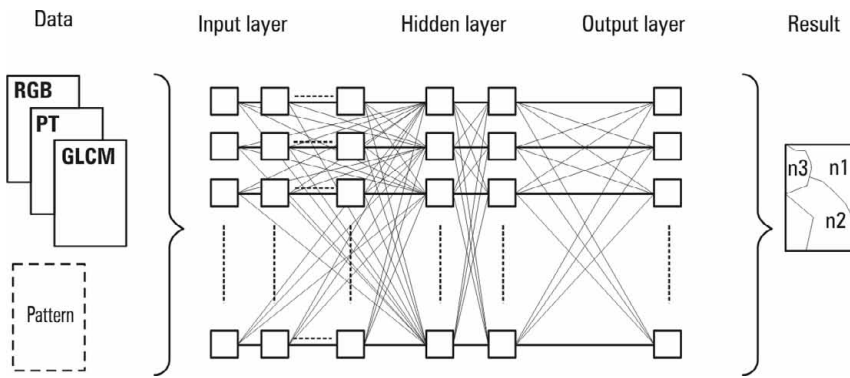
Figure 3.9. The scheme of classification by means of the artificial neural network

of the network after the process of teaching. The feature vector of single pixel is based on the following information:

1. pixel values from separate RGB channels of the airborne photograph,
2. values of texture features calculated with the use of GLCM method on the basis of airborne image in shades of gray,
3. the heights of separate land cover forms calculated on the basis of the difference between the digital surface model (DSM) and the digital terrain model (DTM),
4. values of laser array reflection intensity recorded in the course of airborne laser scanning,
5. number of points reflected on separate levels above the land surface, which describe the forest floor density in the forest stands.

Tables 1 and 2 are annexes to the project and present the visualization of the practice and test sets which are used to assess the 15x15 pixels GLCM mask quality and averaged features (of all classes except for tall vegetation).

3.4.1. Classicfication with the use of the artificial neural network

The clssification was based on artificial neural networks taught by the Standard Back-Propagation method. Fig. 3.9 presents an ideal scheme of classification with the use of the artificial neural network.

When a single input vector constituting a single data portion for the network is processed, the results are compared with expected values and the response error is calculated. Then, the error is back-propagated in the network with the simultaneous weight correction for each vector. The aim of this process is to reduce the input error when the vector is processed again. This cycle is repeated until the error value is lower then the value assumed in the initial condition. Once it happens, the network proceeds to processing the next vector. When the whole process of vector processing is completed, the epoch error is calculated.

The teaching cycle described above is repeated till a satisfactory solution of the problem is achieved.

The network operation verification in its initial stage depends on selecting vectors which differ from the teaching set. Then, the vectors are processed, but the errors are not propagated in this case. The output vector is not given. It is obtained as the outcome of processing. The architecture of the artificial neural network is an important parameter affecting the classification quality.

This architecture covers the number of the hidden layers and the number of neurons within these layers. It has been already documented (Kubik et al., 2006b; Jankowski, 2003) that by using more than three-layered network the classification quality does not improve, but the computational complexity rises significantly. Therefore, the network topology selection is an optimization problem. If the percentage share of correctly recognized pixels in the test set is accepted to be the quality measure, the problem was solved with the use of the evolutionary strategy.

The selection of GLCM mask size for each class

The selection of the mask window size with the use of GLCM method influences the classification quality. Many experiments were carried out to decide which of the four masks considered will be the best one for each land cover class. Masks in sizes 7×7, 15×15, 25×25 and 35×35 pixels were tested for average and non-average of GLCM features. The neural network with a single hidden layer which consists of 9 neurons was used as a classifier. Tab. 3 and 4 available in the appendix contain results of class recognition for classes 1 to 14 for the testing sample. Tab. 5 in the appendix includes training images, the classification standards and the results for the classes of the buildings, streets and railways from 15 to 17. Tab 6 presents the training images, the classification images and the expected results for these classes. A quantitative analysis of the accuracy (Tab. 7, 8, 9 and 10) proved that the texture information has a significant impact on the classification quality, particularly in vegetated areas. In these tables the GLCM mask size which is considered to be the best in a particular class was highlighted in grey. The obtained results prove that the classification quality is better when using a vector which is extended to include non-averaged GLCM features. However, this increases the computational complexity of the problem. In the case of oriented textures, the woods in particular, the use extended features seems to be legitimate. The classification results for masks of 15, 16 and 17 classes are very similar and therefore, the texture features, which are important when the other classes are recognized, do not affect the buildings, streets and railways recognition. Due to the texture character of different classes and their shapes (e.g. street, buildings), there is no general GLCM mask size.

Designing the neural network architecture by using the evolutionary strategy

It is known that the artificial neural network architecture is significant in the process of information processing (Tadeusiewicz, 1993; Rutkowski, 2005; Vonk et al., 1997). The number of neurons on particular layers also influences the network. Too many neurons extend the training process, while too few may result in overfiting of the network. In other words, there may be an effect of a perfect neuron network adjustment to the training data and, simultaneously, there could be loss of capability to generalize the knowledge. It causes a rapid error growth at the network output for test samples.

The network architecture designing is the selection of appropriate layers and numbers of neurons in the layers. Additionally, this process may involve a way in which the neurons connect within the network, rejecting the assumption that neurons connect "with each other". There are many different methods of Network architecture selection – for example the ODB algorithm (Optimal Brain Damage) (Rutkowski, 2005). Because of the fact that the task is a part of the classical task of optimization, it can also be solved with the use of evolutionary methods (Vonk et al., 1997). It is not common, however, to use the operational methods in the selection of the neural network structure. Many authors select the network structure with the use of the trial and error method and they also achieve satisfactory results.

The genetic and evolutionary algorithms, just like neural networks, are the results of the development based on the nature observation. The idea of genetic algorithms is based on the laws of natural selection and inheritance. In nature all the organisms have a specific genetic material in the form of genes located in chromosomes which encode information about genes and enable its passing to the next generations. The new organism comes into being in the process of reproduction. This organism inherits some of its parents' traits through the process called crossover. During the process of passing traits the genotype modification (the genetic material modification) often occurs. It is also known as mutation. If it turns out that the descendant is well adapted, it has a greater chance of passing their genetic material to the next generation than the less adapted individual.

In the digital realization of the optimization task, this idea is based on encoding the problem in the binary form (for the classical genetic algorithm) or in the real form (in case of evolutionary strategies). The environment is defined on the basis of the problem solution by determining so-called adjustment function whose value is maximized during the algorithm operation. The adjustment function determines the degree of the solution correctness. New tasks called generations are created with the use of appropriately defined crossover and mutation operators. The whole evolutionary algorithms family is described in the literature (Rutkowski, 2005; Tadeusiewicz, 1993). The elements below distinguish them from traditional optimization methods, such as the review and analytical methods:

— the evolutionary algorithms do not convert the task parameters directly but their encoded form,
— they search for the optimum solution starting from a group of solutions (so-called initial population), not from an individual solution,
— they use the destination function,
— they use the probabilistic rules, rather than the deterministic ones.

The process of accepting the manner of encoding a structure in a genotype constitutes the first stage in the evolutionary design of the artificial neural network structure. On account of the long process of network teaching, it is possible to resign from incomplete connections between neurons in separate layers – neurons located between the layers are connected with one another. It has been proved that three-layered network is able to define any solution area in multidimensional solution space (Rutkowski, 2005). It enables to limit the searching space to the maximum of three hidden layers. Taking into consideration the rapid growth of calculations connected with the use of extended networks, it was assumed that the number of neurons on one layer will not exceed 10. These assumptions enable the chromosomes of a single solution to reduce to three natural code numbers, the number of chromosomes on separate layers. The modified evolutionary strategy used in calculations ($\mu+\lambda$) is wider described in literature (Rutkowski, 2005; Vonk et al., 1997). Fig. 3.10 presents a modular scheme of this method.

The algorithm starts with drawing the initial parental population P containing μ individuals and assessing their adjustment (the network is taught on the basis of the teaching set, the testing set is classified and finally classification quality is evaluated). The classification quality measure 2.36, defined in chapter 2.3, was assumed as the adjustment function. Then, via reproduction a temporary population T, containing λ individuals, is created. The process of reproduction is based on a repeated random selection of λ individuals from a population P. Individuals of population T are subject to crossover and mutation and as a result, a descendant population $\mathbf{O}$ is obtained. Next, an assessment of adjustment of the $\mathbf{O}$ population individuals is carried out and μ well-adjusted individuals are chosen from both populations $P \cup \mathbf{O}$ constituting the new parental population P. This process is repeated an initially assumed number of iterations (the assumed number of generations). The best individual from the last generation is accepted as the solution.

The ($\mu + \lambda$) strategy contains an automatic adjustment of the mutation scope which is very significant in the new searching solutions. Every individual, apart of genes which include the encoded x-task parameters, also has a chromosome σ where values of standard deviations used during mutation are stored. Both chromosomes are subject to operations described above. Thus, the scope of searching for new solutions is regulated and it should diminish when it approaches the optimum solution.

The operation of the crossing operator consist in drawing two individuals according to the formula 3.12,
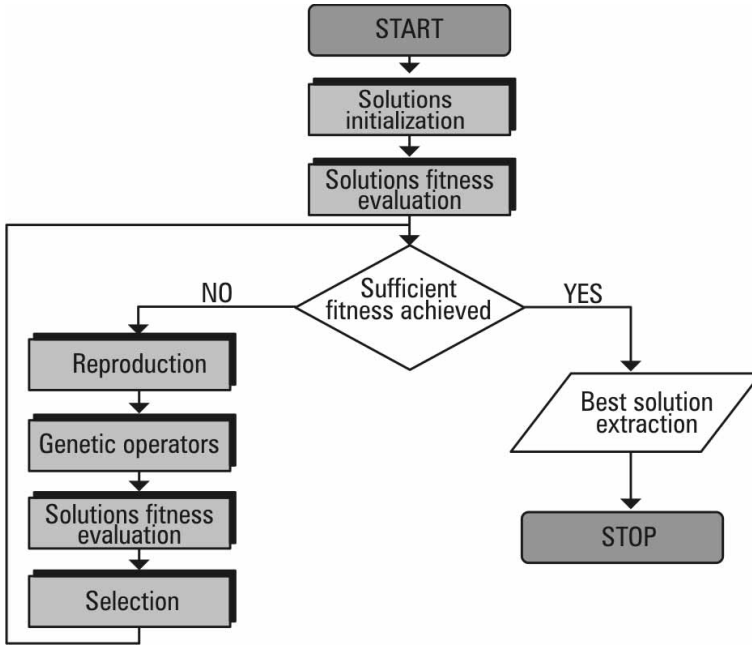
Figure 3.10. Scheme of the evolutionary strategy algorithm $(\mu + \lambda)$

$$(x^1, \sigma^1) = \left(\left[x_1^1, \ldots, x_n^1 \right]^T, \left[\sigma_1^1, \ldots, \sigma_n^1 \right]^T \right)$$
$$\text{and } (x^2, \sigma^2) = \left(\left[x_1^2, \ldots, x_n^2 \right]^T, \left[\sigma_1^2, \ldots, \sigma_n^2 \right]^T \right)$$

and then exchanging the values of their genes according to the formula:

$$(\hat{x}, \hat{\sigma}) = \left(\left[x_1^{q_1}, \ldots, x_n^{q_n} \right]^T, \left[\sigma_1^{q_1}, \ldots, \sigma_n^{q_n} \right]^T \right), \tag{3.12}$$

where: $\quad q_i = 1$ lub $q_i = 2$.

The mutation operator acts on a single individual. As the first the chromosome σ is subjected to mutation according to formula 3.13.

$$\hat{\sigma}_i = \sigma_i \exp\left(\acute{\tau} N(0,1) + \tau N_i(0,1) \right), \tag{3.13}$$

where: $\quad i = 1, \ldots, n,$
$n -$ chromosome length,
$N(0,1) -$ random number from the normal distribution, drawn once for the whole chromosome,
$N_i(0,1) -$ number from the normal distribution drawn once for the whole gene,
τ i $\acute{\tau} -$ parameters which influence the algorithm convergence.

Table 3.4. Selection of the optimal neural network topology for classification of land cover classes.

Class	Best topology	Adjustement function [%]
1	10 3 10	100
2	0 10 10	99.02
3	10 10 10	94.05
4	0 10 10	96.24
5	10 10 3	92.86
6	1 10 10	92.86
7	10 5 1	99.59
8	4 5 10	96.09
9	10 5 8	99.97
10	10 10 2	99.47
11	1 10 1	99.74
12	10 10 2	99.44
13	0 7 4	97.03
14	10 10 5	96.49
15	10 3 10	90.33
16	10 5 10	90.33
17	6 1 8	98.03

To calculate the parameters τ and $\acute{\tau}$, the following formulas can be applied (Rutkowski, 2005):

$$\acute{\tau} = 1/\sqrt{2n}, \quad \tau = 1/\sqrt{2\sqrt{n}} \tag{3.14}$$

Parameters $\hat{\sigma}_i$ influence the x_i value change:

$$\hat{x}_i = x_i + [\hat{\sigma}_i N_i(0,1) \times 10] \tag{3.15}$$

The algorithm modification consist in on formulating such mutation operators that the solutions space is limited to natural numbers. It was achieved by increasing by one order of magnitude the product of mutation coefficient and a random number and by using their integer part to modify the x_i parameter.

Many experiments were carried out in order to select the best neural network topology for the image classification of land cover classes. The process of selection was carried out for eight generations. The initial population μ and the descendent population λ equal 10. For each land cover class the best construction of the neural network was determined. The process of training was carried out on the training samples and the adjustment assessment was done on the test samples. The results are presented in the Tab. 3.4.

Land cover classification of the Widawa valley with the use of neural networks with allowance for the flow resistance

The last stage of the image classification with the use of the artificial neural networks is to construct the classifier through the process of training with the use of the training samples which contain data chosen in the previous experiments. The process of recognition was carried out individually for each class, which means that for each of the seventeen classes the individual network was trained, which could indicate points belonging or not belonging to the class being recognized. The applied networks' architectures are presented in the Tab. 3.4. Non-average GLCM features were taken into consideration in the vector. The GLCM masks' sizes indicated in a Tab. 9 were used. In the case of neural networks, the process parameters are:

— training method – to choose from: standard back-propagation method, rprop, QuickProp,
— number of neurons on the hidden layers – maximum three layers,
— number of training cycles,
— colour palette used for classification.

The data for classification should be loaded after the network's training. The data format is similar to the training data, however, there is no demand for the initial standard. The visualization of the neural network depends on:
— in the case of one class recognition – a decision about belonging to the class, if the value on the output neuron equals or is higher than 0.5,
— in the case of multiple-class recognition – a decision is taken on the basis of the majority vote of the value on the network output. One neuron of the output layer is assigned to each class. The decision depends on classifying a pixel into the class whose neuron has the greatest output value, however, not smaller than 0.2. If the values on any of the output neurons did not meet the above condition – lack of recognition was marked in black.
Recognition of all the classes for the whole study area was carried out. The network was trained with the use of the standard back-propagation method within 2000 cycles. The obtained results for single recognition were put together in one colour image, presented in Fig. 3.11. The quantitative assessment of recognition quality for each class was carried out on the basis of training samples (Tab. 3.5).

By analyzing data presented in Tab. 3.5 one can notice a poor quality of image classification for classes 3, 5 and 6, i.e. for some types of forest. These results suggest that the assumed classification detail might have been too high. The image classification quality of other classes can be assumed good. It should be remembered that the verification was carried out on a small testing area only. Moreover, the quality of photographic material (problems with tonal adjustment) and the digital terrain model caused that incorrectly classified areas can be noticed in some places when comparing the achieved results with the image mosaic. To sum up, the majority of areas was classified at a satisfactory level, just the recognition of some kinds of forests failed. However, the quality of the image classification can

Table 3.5. Compilation of quality measures for classification based on artificial neural networks for the test set

Class number	Measure			
	$\hat{\kappa}$	u_i	p_i	d
1	1	1	1	1
2	0.9972	0.9954	1	1
3	0.3458	0.2101	0.6481	0.9300
4	0.9104	0.8241	0.9867	0.9921
5	0.3110	0.7204	0.3400	0.8674
6	0.2842	0.2516	0.4442	0.9240
7	0.9991	0.9948	0.9940	0.9999
8	0.7848	0.7210	0.9800	0.9917
9	0.9997	1	0.9981	1
10	0.9999	0.9990	0.9778	0.9978
11	0.9896	0.9958	0.9842	0.9995
12	0.9961	0.9899	0.9986	1
13	0.9608	0.9570	0.9569	0.9993
14	0.8462	0.7802	0.9524	0.9789
15	0.9161	0.9875	0.9207	0.9824
16	0.9738	0.9989	0.9718	0.9699
17	0.9640	0.9707	0.9974	0.9540

be improved by replacing the amateur aerial images with professional photogrammetric imageries (made together with laser scanning at small time interval) and by using digital terrain model and digital surface model, which are more efficient with respect to point filtering for forest areas. Further research on vegetation density in vertical section, on the basis of laser scanning data, seems to be very promising.
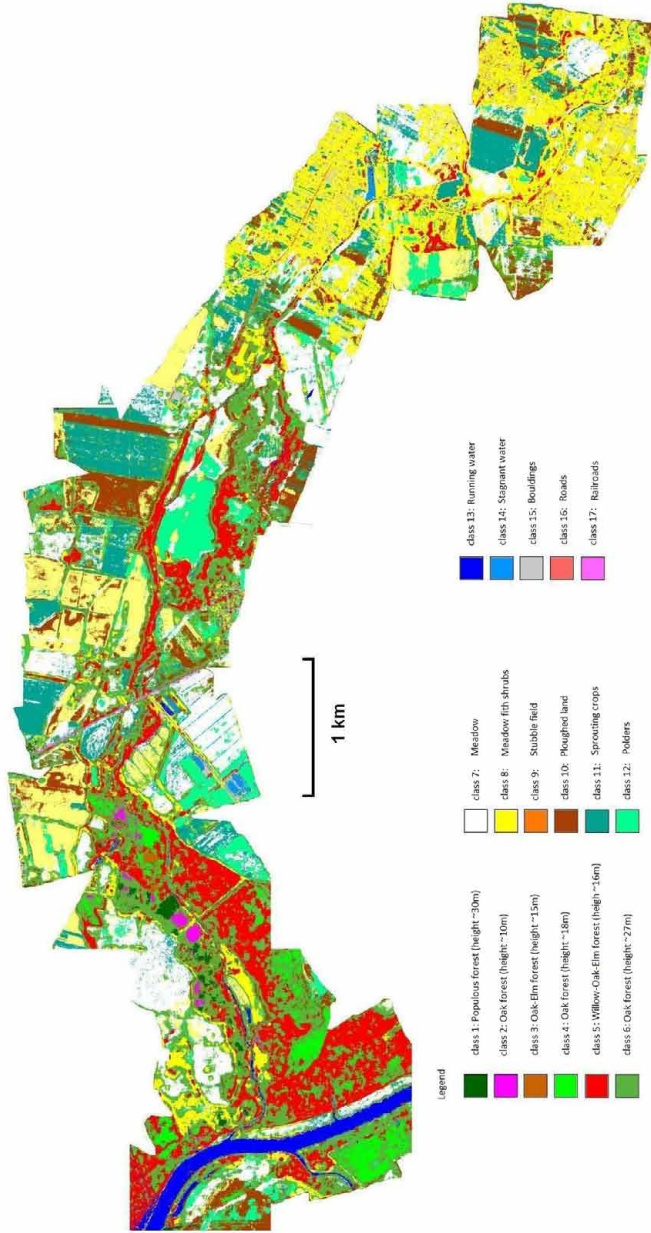
Figure 3.11. Land cover map of the study area showing flow resistance

3.4.2. Image classification with the maximum likelihood method

In the statistic approach described in section 2.1.1, called in literature the maximum likelihood method or the Bayes' parametric algorithm case, to create the classifier it is necessary to assume a known type of distribution and estimate this distribution parameters on the basis of the training samples and a'priori likelihood value of the class membership. The multi-dimensional normal distribution model was used in the test. A visual histogram analysis (one-dimensional) of the training samples was carried out before making the decision. RGB and GLCM data have the histogram characteristics similar to the normal distribution. However, the height model (DM) for classes 7–17 and intensity (INT) data for classes 13–14 certainly do not have the normal distribution. The above conclusion is confirmed by the fact that the attempt of data estimation with the normal distribution results a peculiar matrix of features covariance and, thus, it eliminates the possibility of carrying out the image classification. Despite all these restrictions, an attempt was made to assess the usefulness of the method in image classification in order to evaluate the roughness coefficients. The results of the experiments were compared with the results obtained with the use of artificial neural network in the previous chapter 3.4.1.

First, classes 1 to 12 were recognized. The multi-dimensional normal distribution of features was assumed in the class recognized and the same model was assumed for other areas that constituted one common class. The method is similar to assumed image classification with the artificial neural network described in chapter 3.4.1 and depends on recognition of areas belonging to one class during one experiment. Tab. 3.6 presents the achieved recognition quality measures (according to section 2.3).

When analyzing the obtained measures, Tab. 3.6, and comparing them with the results obtained with the artificial neural network, it can be stated that the image classification with the use of the maximum likelihood algorithm is not successful. The achieved measures prove that there is no correct recognition (classes: 3, 4, 6, 7, 8, 9, 12), or there is little conformity with the expected outcome(classes: 1, 2, 5, 10, 11). This fact is confirmed by the image classification of a part of the study area (square no 6), compiled in Fig. 3.12 with the result of the neural network recognition.

The next experiment consisted in classification of all the classes of tall vegetation (classes 1–6) assuming the multidimensional normal distribution model for features in each class. Fig. 3.13 presents visualization of the recognition with a use the maximum likelihood method for the test samples. Tab. 3.7 presents the calculated quality measures.

Comparison of the results in Fig. 3.13 and Tab. 3.7 with the results of classification of the same classes using the artificial neural network method speaks in favour for the second method. Fig. 3.14 presents the results of classification of

Table 3.6. Compilation of quality measures for classification of classes 1 to 12
with maximum likelihood method for the test set.

Class number	Measure			
	p_i	u_i	$\hat{\kappa}$	d
1	1.00000	0.20921	0.32944	0.94352
2	1.00000	0.01800	0.03292	0.92985
3	NAN	0.00000	0.03292	0.92854
4	NAN	0.00000	0.03292	0.92854
5	1.00000	0.00160	0.00297	0.92868
6	1.00000	0.00000	-0.00611	0.92540
7	NAN	0.00000	0.03292	0.92854
8	NAN	0.00000	0.03292	0.92854
9	NAN	0.00000	0.00000	0.92857
10	1.00000	0.05120	0.09109	0.93223
11	1.00000	0.06840	0.11999	0.93346
12	NAN	0.00000	0.00000	0.92857
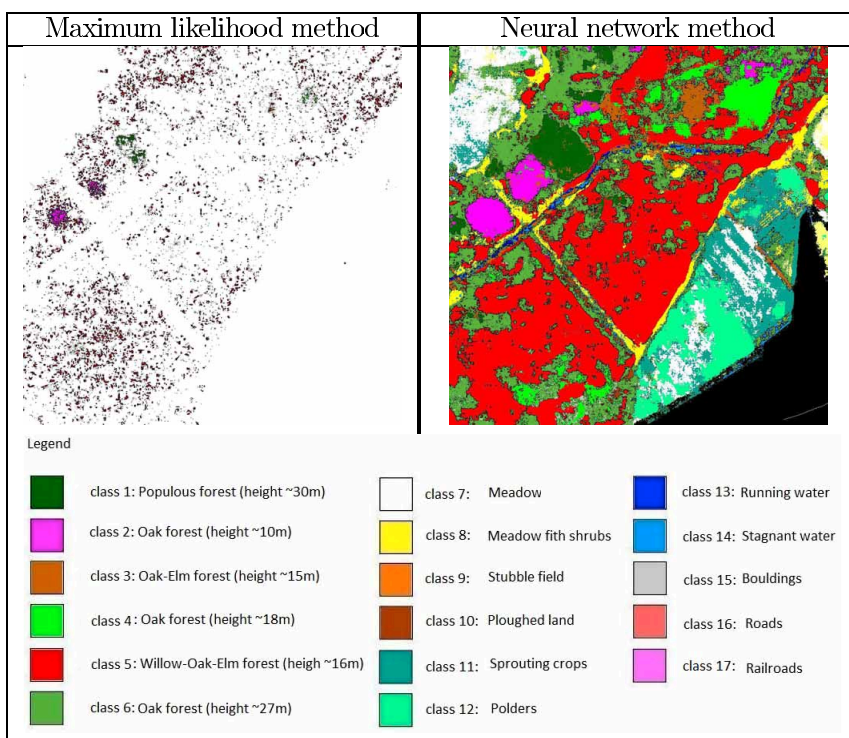
Figure 3.12. Comparison of image classification using maximum likelihood method
with the artificial neural network method (square 6 of the study area)

Class	Feature vector	Expected result	Achieved result
1: Populous forest (30m)			
2: Oak forest (10m)			
3: Oak-Elm forest (15m)			
4: Oak forest (18m)			
5: Willow-oak-Elm forest (16m)			
6: Oak forest (27m)			
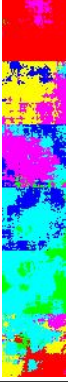
Figure 3.13. Visualization of the test vectors classification for classes 1 to 6 using the maximum likelihood method

Table 3.7. Compilation of quality measures for classification of classes 1 to 6 with maximum likelihood method for the test set

Class number	Measure				
	p_i	u_i	$\hat{\kappa}$	$\hat{\kappa}_w$	d
1	0.90600	0.76962			
2	0.58400	0.74149			
3	0.54320	0.54363	0.42696	0.53906	0.52247
4	0.34760	0.51787			
5	0.71080	0.36399			
6	0.04320	0.10485			

Maximum likelihood	Neural network
Airborne photograph	Legend
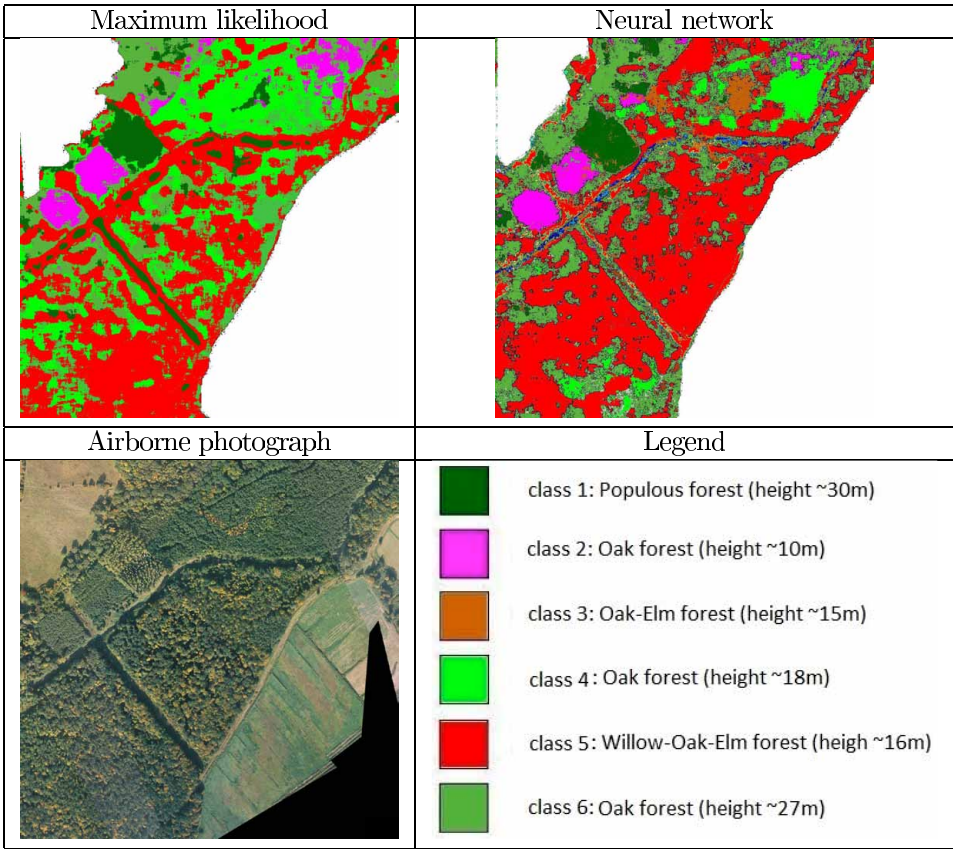
Figure 3.14. Comparison of image classification using maximum likelihood method
with the artificial neural network method (square 6) and tall vegetation

classes 1-6 with the maximum likelihood method and the artificial neural network
method with a picture for square 6 of the study area.

Visual comparison of the results of classification results with the aerial image
suggests also that the neural network method is more reliable for this task.

To sum up, the maximum likelihood method, which assumes the normal feature
distribution in classes, gives results which are significantly worse than those from
the artificial neural network method. This may be caused by the application of the
normal distribution model in that method, whereas it is not necessary in the case
of the neural network classification where the distribution model is not explicitly
determined.

3.5. Transformation of the roughness coefficients to hydrodynamic models

Creation of a high quality hydrodynamic model requires a precise geometric description of the discharge area as well as the characteristics of the surface roughness. In the case of systems using two-dimensional model (e.g. SMS, MIKE-11, MIKE-21) the data is entered in the form of a discrete grid with the resistance coefficients attributed to meshes. This so-called "surface" approach results in that the map of roughness classes which is achieved by the automatic classification (Fig. 3.11) and the complementary digital terrain model may be directly introduced to this type of the system. The model developed for the purpose of this work as well as the cover map have 1x1 m resolution which may be problematic because of the calculation effort connected with the process of the hydrodynamic modeling. Thus, a reduction of the grid resolution should be taken into consideration before putting it into the model.

The process of putting in a digital terrain model with resistance coefficients can be technically carried out with the use of GIS systems (e.g. ARC-GIS). The automatic vectorization of the resistance coefficients map is required. The 1-D models are commonly used in the engineering practice, for example in the HEC-RAS model. To describe geometry, this model uses cross-sections which should be perpendicular to a dominating direction of the water stream (Radczuk et al., 2001). In such a model the coefficients are put in segment by segment along the section or in the form of equivalent roughness separately for left or right floodplain and the river bed (Sobota, 1994). However, the river bed area is always treated as homogeneous in its section with respect to the flow resistance. Transformation of the geospatial data to the HEC-RAS model in version 4.0 may be performed using geospatial data import function in the *.geo format. It is essential to transform the record of the surface roughness classes into data of valley cross-sections. It is carried out on the basis of digital terrain model, the roughness class map as well as a table that assigns a specific resistance coefficient to each class through the process of resampling the height value for the indicated section and in accordance with one of the methods described in Chapter 1.2.2. Fig. 3.15 presents the visualization of a part of the digital terrain model of the river valley with marked sections and the watercourse axis.

The export data file of the HEC-RAS package is a text file. It contains sections describing locations of the watercourse axes, coordinates of points in the cross-sections along with the resistance coefficients. The detailed format specification may be found in the appendix to the package usage (HEC-RAS, 2006). The process of loading the data files to the HEC-RAS project is carried out through the geometric data import module (the geometric data window, the option: "Import geometry data – format GIS" (Fig. 3.16).

Fig. 3.17 presents an exemplary section of the Widawa valley with information about roughness.
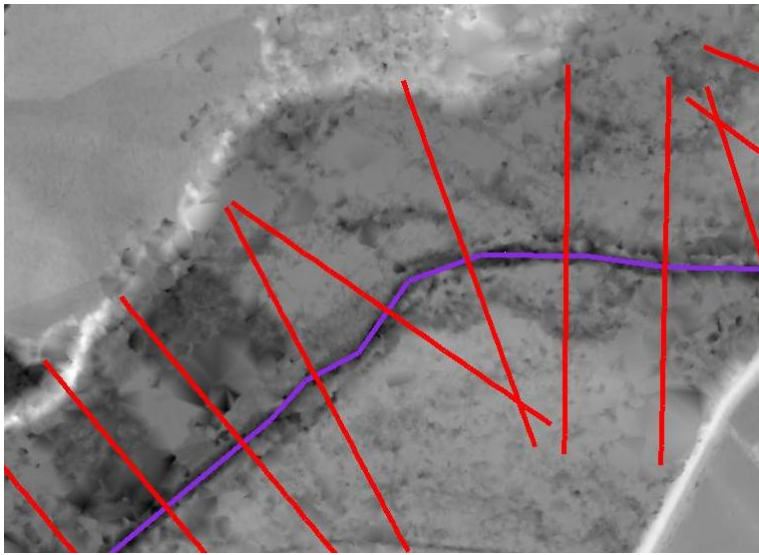
Figure 3.15. An exemplary part of the digital model of the river valley with marked location of the sections and the watercourse axis
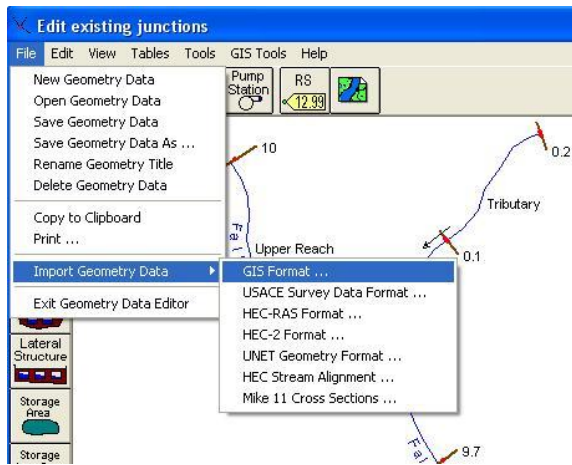
Figure 3.16. The option of the geometric data import in the HEC-RAS package

The minimum interval between sections is limited to DTM resolution and the land cover map. Thus, it is possible to generate data of very high detail (Fig. 3.18).

To sum up, the transfer of the assessed discharge resistance and the digital terrain model to different hydrodynamic models is possible to perform. It is necessary
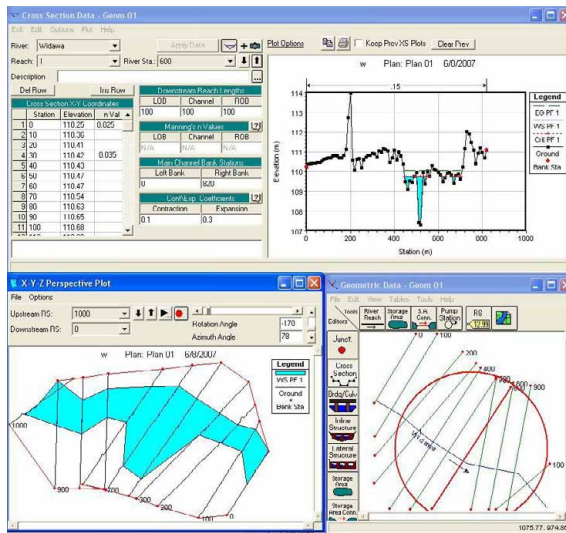
Figure 3.17. An exemplary section of the Widawa valley with information about the roughness imported into HEC-RAS model
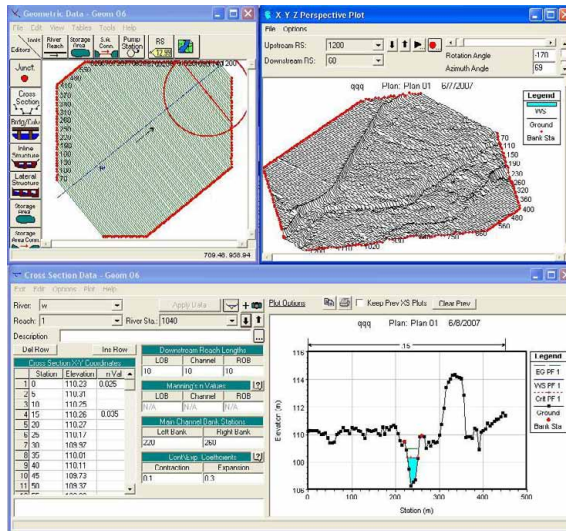
Figure 3.18. An exemplary import of detailed data into HEC-RAS system

to enter the rest of the required data (such as the hydrological information, the information about the channel and embankment location, etc.) before modeling. The laser scanning method does not provide information about the real channel

shape. Information on the river bed roughness also needs to be completed by
consulting other sources. On account of economy, the use of digital models and
the high resolution roughness coefficients maps is questionable in the case of 1D
models. A great amount of data is lost at the transformation stage. The method-
ology of geospatial data generation for the purpose of hydrodynamic modeling,
discussed in this paper, should be associated with the development of 2D and 3D
models which, due to the increasing calculation capacity of computers, may shortly
replace 1D models.

Chapter 4

Summary and conclusions

Summing up, there is a possibility of automatic recognition of surface roughness classes on the basis of integrated data from different sources. However, the quality and detail of such classification is significantly influenced by the applied measuring techniques and the selection of classification methods and parameters. Satisfactory results can be achieved by combining laser scanning data with airborne images. Such data integration from different sensors, in other words the process of combining information from many different sources, is up-to-date. Moreover, airborne laser scanning as the main technology of data acquisition, which are used to create detailed terrain models, may also be used as a source of information on the land cover classification. The presented method of automatic recognition of homogeneous areas with respect to the flow resistance was based on the supervised classification techniques. The first stage is to indicate a minimum of two small areas (the training and testing areas) for each class as their representation, which is used to create the classifier and for quantitative assessment of accuracy. These areas should be surveyed paying special attention to their hydraulic characteristics. For that purpose it is recommended to carry out a reconnaissance. The resistance parameters of class samples can be determined on the basis of tables (e.g., Ven Te Chow) or in case of tall vegetation areas − on the basis of measured geometrical parameters of trees and bushes. These parameters are the average diameter of tree trunk (in case of bush: the macro structural approach) and the average gauge. The classifier's model should be created on the basis of the training samples after data integration on the basis of airborne laser scanning and airborne images. To create the classifier, it is necessary to determine parameters of features extraction (the GLCM mask size) and of the classification (topology of the hidden layers of a neural network, the distribution type of features density in classes and the `a priori` probability in the likelihood algorithm). The determined parameters are not universal. They depend on the imagery scale and the character of the recognized classes. They need to be selected for every measuring campaign. The test samples are used to assess the classification quality. In the case of a positive recognition assessment it is possible to classify the whole study area. The roughness map obtained as a result of classification and the complementary DTM constitute the geometric base of the hydrodynamic modeling. Depending on the applied system, the process of entering the data may differ. The procedure of data transforming into one-dimensional HEC-RAS model is presented in this work. The suggested system of land cover classification for application in hydrodynamic modeling can
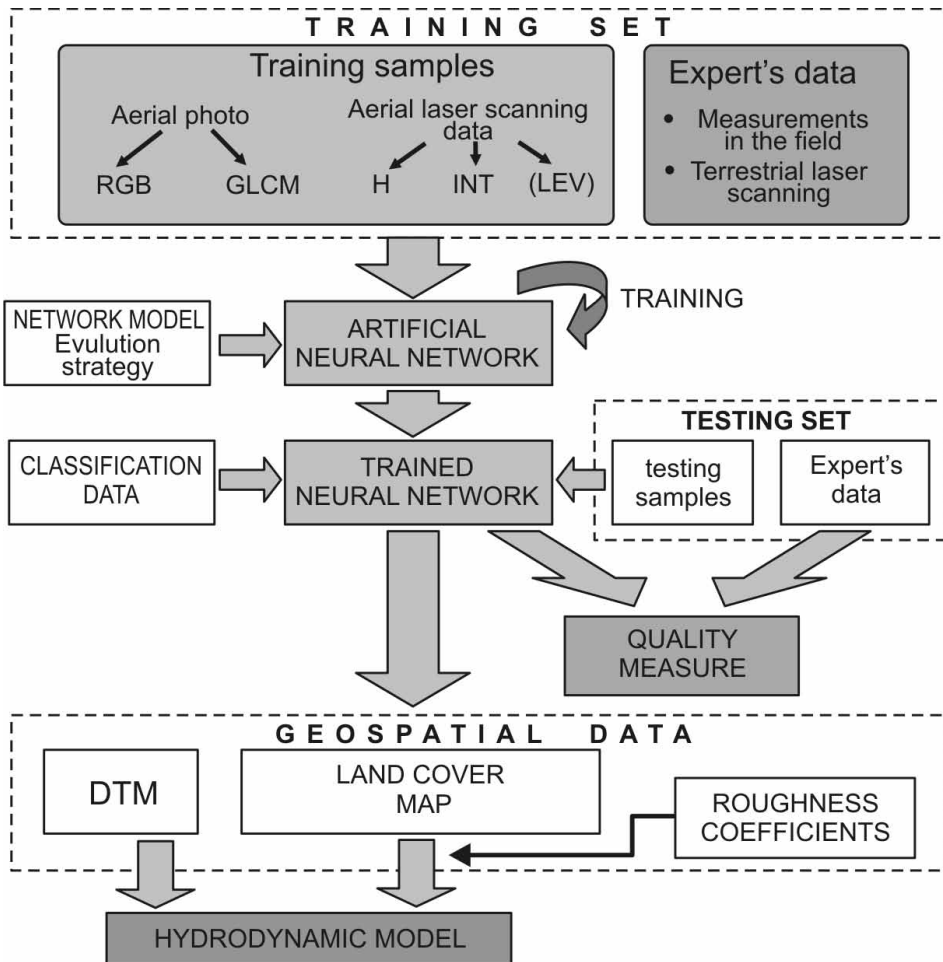
Figure 4.1. Classification system scheme of the land cover for the use of hydrodynamic modeling

be presented in the form of a scheme (Fig. 4.1). The suggested method of automatic transformation of the geometric data and terrain features (the roughness classes) into hydrodynamic models should be connected with their improvement and development.

On the basis of the presented research it is possible to formulate the following detailed conclusions:

— The image classification with the maximum likelihood method, assuming the normal distribution model as features density function in a class, gives substantially worse results than the artificial neural network method and, moreover,

is impossible to apply in the case of data that do not conform to the normal distribution.

— The best results of image classification were achieved with the neural classifier assuming recognition of each class with the use of separate network.

— In the case of maximum likelihood classifier the application of the same approach (separate classifier for each class) gives no positive results – practically no recognition. However, a simultaneous classification of all classes with the use of this method gave acceptable results, not worse than the results obtained with the use of the artificial neural network method.

— The effectiveness of recognition highly depends on data quality and selection of the classification parameters as well as on the manner of features extraction (the selection of mask size in the GLCM method, the features selection, the neural network topology).

— Slightly better results can be achieved by allowing non-averaged GLCM parameters in the features vector.

— The GLCM mask size as well as the neural network topology should be determined individually for each class.

— In the process of selecting the best topology of hidden layers of neural networks, the evolutionary strategy gives the satisfactory results.

— GLCM features do not significantly affect the class recognition of buildings, roads and railways.

List of Figures

List of Tables

Bibliography

Adamczyk, J., Będkowski, K., 2005. Metody cyfrowe w teledetekcji. Wydawnictwo SGGW.

Aplin, P., Atkinson, P. M., 2001. Sub-pixel land cover mapping for per-field classification. International Journal of Remote Sensing 22 (14), 2853–2858.

Aschoff, T., Thies, M., Spiecker, H., 2004. Describing forest stands using terrestrial laser scanning. International Archives of the ISPRS, Istanbul, Turkey.

Atkinson, P., Lewis, P., 2000. Geostatistical classification for remote sensing: an introduction. Computers and Geosciences 26 (4), 361–371.

Barilotti, A., Turco, S., G., A., 2006. Lai determination in forestry ecosystem by lidar data analysis. Workshop on 3D Remote Sensing in Forestry, 14-15 February, Veinna, Austria. pp. 248–252.

Borkowski, A., 2005. Filtracja danych lotniczego skaningu laserowego z wykorzystaniem metody aktywnych powierzchni. Polskie Towarzystwo Informacji Przestrzennej, Rocznik Geomatyki tom III, zeszyt 4, 35–42.

Borkowski, A., 2006. Lotniczy skaning laserowy jako metoda pozyskiwania danych dla potrzeb modelowania hydrodynamicznego. Aktualne problemy rolnictwa, gospodarki żywnościowej i ochrony środowiska. AR Wrocław, 129–136.

Borkowski, A., Gołuch, P., Mokwa, M., Tymków, P., 2006a. Wykorzystanie lotniczego skaningu laserowego do budowy numerycznego modelu terenu doliny rzeki widawy. Problemy Hydrotechniki. Złotniki Lubańskie, pp. 171–178.

Borkowski, A., Gołuch, P., Wehr, O., Schiele, M., Thomas, M., 2006b. Airbone laser scanning for the purpose of hydrodynamic modelling of widawa river valley. Reports on Geodesy 2(77), 85–94.

Bretschneider, H., Schultz, A., 1985. Anwendung von fliessformeln bei naturnahem gewasserausbau. Tech. Rep. Heft 72.

Bubnicki, Z., 1969. Least interval pattern recognition and its application to control systems. Vol. 21 of IFAC Congress. Warszawa.

Buddenbaum, H., Seeling, S., 2006. Estimating structural forest attributes using high resolution, airborne hyperspectral and lidar imagery. Workshop on 3D Remote Sensing in Forestry, 14-15 February, Veinna, Austria. pp. 253–257.

Campbell, J., 1996. Introduction to Remote Sensing, 2nd Edition. Taylor&Francis, London.

Chang, H.-C., Kopaska-Merkel, D. C., Chen, H.-C., 2002. Identification of lithofacies using kohonen self-organizing maps. Computers and Geosciences 28 (2), 223–229.

Charaniya, A., Manduchi, R., Lodha, S., 2004. Supervised parametric classification of aerial lidar data. Conference: Computer Vision and Pattern Recognition.

Chasmer, L., Hopkinson, C., Treitz, P., 2004. Assessing the three-dimensional frequency distribution of airborne and ground-based lidar data for red pine and mixed deciduous forest plots. Int. Archives of Photogrammetry, Remote Sensing and Spatial Information Sciences XXXVI, part 8/W2, 66–70.

Chow, V. T., 1959. Open channel hydraulics. McGraw Hill, New York.

Cichocki, A., Unbehauen, R., 2002. Neural networks for optimization and signal processing. Wiley, New York.

Cichosz, P., 2000. Systemy uczące się. Wydawnictwo Naukowo-Techniczne, Warszawa.

Ciołkosz, A., Miszalski, J., Olędzki, J., 1999. Interpretacja zdjęć lotniczych. Wydawnictwo PWN Warszawa.

Dąbkowski, S., Pachuta, K., 1996. Roślinność i hydraulika koryt zarośniętych. Wydawnictwo Instytutu Melioracji i Użytków Zielonych.

Devijver, P., Kittler, J., 1982. Pattern Recognition: A statistical Approach. Prentice Hall, London-Toronto-Sydney.

Ducic, V., Hollaus, M., Ullrich, A., Wagner, W., Melzer, T., 2006. 3d vegetation mapping and classification using full-waveform laser scanning. Workshop on 3D Remote Sensing in Forestry, 14-15 February, Veinna, Austria. pp. 211–217.

Duda, R., Hart, P., 1973. Pattern Classification and Scene Analysis. John Wiley&Sons, New York-London-Sydney.

Duda, R. O., 2001. Pattern classification. John Wiley & sons, New York.

Fleiss, J. L., 1981. Statistical Methods for Rates and Proportions, second edition Edition. Vol. 20. John Wiley & Sons, New York.

Foody, G. M., 1960. A coefficient of agreement for nominal scales. Educational and Psychological Measurement 20, 37–46.

Froehlich, D., 2002. Two-dimentional Depth-averaged Flow and Sediment Transport. University of Kentucky Research Foundation.

German, G. W. H., Gahegan, M. N., 1996. Neural network architectures for the classification of temporal image sequences. Computers and Geosciences 22 (9), 969–979.

Gierczak, J., 1998. Metody odwzorowania współczynników szorstkości terenów zalewowych na przekrój obliczeniowy, 41–48.

Gil, J., 2006. Przykłady zastosowań sieci neuronowych w geodezji. Oficyna Wydawnicza Uniwersytetu Zielonogórskiego, Zielona Góra.

Gołuch, P., Kałuża, T., Leśny, J., Szoszkiewicz, K., 2004. Teledetekcyjna ocena struktury roślinności obszaru wisły środkowej na podstawie obrazów satelity landsat 7 etm+. No. 3(1–2) in Acta Scientarum Polonorum Geodesia et Descriptio Terrarum. pp. 57–69.

Gołuch, P., Markowski, J., Mokwa, M., 2000. Wykorzystanie nmt do wyznaczania stref zagrożenia powodziowego. XX International School of Hydraulics, Współczesne problemy hydrauliki wód śródlądowych. Kraków, pp. 71–76.

Grocki, R., Czamara, W., 2001. Metody ograniczania skutków powodzi.

Wydawnictwo RM Wrocław.

Hastie, T., Tibshirani, R., Friedman, J., 2001. The Elements of Statistical Learning. Data Mining, Inference and Prediction. Springer-Verlag, New York-Berlin-Heidelburg.

HEC-RAS, 2006. River Analysis System, User Manual, Version 4.0.0 Beta.

Hoppner, F., Klownn, F., Runkler, T., 1999. Fuzzy cluster analysis, methods for classification, data analysis and image recognition. Wiley.

Hubert-Moy, L., Cotonnec, A., Le Du, L., Chardin, A., Perez, P., 2001. A comparison of parametric classification procedures of remotely sensed data applied on different landscape units. Remote Sensing of Environment 75 (2), 174–187.

Iwaniak, A., Kubik, T., Paluszyński, W., Tymków, P., 2005. Classification of features in high-resolution aerial photographs using neural networks. XXII International Cartographic Conference A Coruna (Spain).

Iwaniak, A., Kubik, T., Paluszyński, W., Tymków, P., 2006. Feature extraction in high-reolution raster images using neural network. 8th Bilateral Geodetic Meeting Poland-Italy, Wrocław 22-24 June.

Jankowski, N., 2003. Ontogeniczne sieci neuronowe. Akademicka Oficyna Wydawnicza, Warszawa.

Katzenbeisser, R., 2003. Toposys gmbh technical note, http://www.toposys.de/pdfext/.

Kałuża, T., 1995a. Metody określania współczynnika oporu porostu na podstawie parametrów geometrycznych roślin. Współczesne problemy hydrauliki wód śródlądowych, XV Ogólnopolska szkoła hydrauliki. Wrocław-Trzebieszowice, pp. 225–231.

Kałuża, T., 1995b. Określanie współczynnika szorstkości w wybranych przekrojach rzeki warty. Współczesne problemy hydrauliki wód śródlądowych, XV Ogólnopolska szkoła hydrauliki. Wrocław-Trzebieszowice, pp. 233–239.

Kałuża, T., 1996. Metody matematycznego opisu struktury roślinnej terenów zalewowych. Współczesne problemy hydrauliki wód śródlądowych, XVI Ogólnopolska szkoła hydrauliki. Grodno k. Międzyzdrojów, pp. 153–158.

Kałuża, T., 1999. Badania modelowe współczynnika oporów liniowych koryta z kępami krzewów. Współczesne problemy hydrauliki wód śródlądowych, XIX Ogólnopolska szkoła hydrauliki. Frombork, pp. 199–204.

Koch, B., Heyder, U., Straub, C., Weinacker, H., 2006. 3d data for forest and environmental planning. Workshop on 3D Remote Sensing in Forestry, 14-15 February, Veinna, Austria. pp. 1–14.

Kot, A., Szymkiewicz, R., 2002. Uproszczone liniowe modele transformacji fali w korycie rzecznym. Tech. Rep. Zeszyt 20, Warszawa.

Kouwen, N., Unny, T., 1973. Flexible roughness in open channels.

Kubik, T., Paluszyński, W., Iwaniak, A., Tymków, P., 2004. Supervised classification of multi-spectral satellite images using neural networks. Proceedings of the 10th IEEE International Conference on Methods and Models in Automation and Robotics. pp. 769–774.

Kubik, T., Paluszyński, W., Iwaniak, A., Tymków, P., 2005. Image processing for

gis applications supported by the use of artificial neural netwroks. Tenth International Symposium on Artificial Life and Robotics. AROB 10th '05 Sugisaka Masanori. pp. 616–619.

Kubik, T., Paluszyński, W., Iwaniak, A., Tymków, P., 2006a. Land-cover/land-use mapping based on color feature extraction. Eleventh International Symposium on Artificial Life and Robotics. AROB 11th'06 Sugisaka Masanori. pp. 735–738.

Kubik, T., Paluszyński, W., Iwaniak, A., Tymków, P., 2006b. Zastosowanie sztucznych sieci neuronowych w procesie tworzenia regionalnych systemów informacji przestrzennej w skali 1:50000 na podstawie obrazów satelitarnych i zdjęć lotniczych (Praca w druku). Monografie AR Wrocław.

Kubrak, J., Nachlik, E., 2003. Hydrauliczne podstawy obliczania przepustowości koryt rzecznych. Wydawnictwo SGGW Warszawa.

Kukuła, J., Magnuski, K., Miś, R., Ważynski, B., Żółciak, E., 1997. Zagadnienia praktyczne z urządzania lasu, część 1, inwentaryzacja lasu i plany urządzania lasu. Tech. rep.

Kurzyński, M., 1997. Rozpoznawanie obiektów Metody statystyczne. Oficyna Wydawnicza Politechniki Wrocławskiej.

Kwiatkowski, W., 2001. Metody automatycznego rozpoznawania wzorców. Wojskowa Akademia Nauk, Warszawa.

Landis, J., Koch, G. G., 1977. The measurement of observer agreement for categorical data. Biometrics 33, 159–174.

Linh, T., 2004. Współczesne generacje sztucznych sieci neuronowych i ich zastosowania w wybranych problemach klasyfikacji. Oficyna Wydawnicza Politechniki Warszawskiej, Warszawa.

Lucas, R., Lee, A., Bunting, P., Williams, M., 2006. Forest reconstruction from lidar and casi data: A case study from australia. Workshop on 3D Remote Sensing in Forestry, 14-15 February, Veinna, Austria. pp. 184–188.

Majewski, W., 2005. Progress in hydraulic reasearch during past 25 years. Hydraulic and Environmental Problems in Open Channel Flows in View of Water Framework Directive, XXV International School of Hydraulics. Debrzyno, pp. 23–31.

Meyer-Bäse, A., 2004. Pattern Recognition for Medical Imaging. Elsevier Academic Press, San Diego USA.

Mikrut, S., Marmol, U., Będkowski, K., 2006. Generowanie nmt i nmpt obszarów z pokrywą roślinną na podstawie danych lidarowych. Archiwum Fotogrametrii, Kartografii i Teledetekcji.

Miller, D. M., Kaminsky, E. J., Rana, S., 1995. Neural network classification of remote-sensing data. Computers and Geosciences 21 (3), 377–386.

Mokwa, M., 2003. Ocena przepustowości doliny Widawy dla przeprowadzenia części przepływów powodziowych Odry. Wydawnictwo Akademii Rolniczej we Wrocławiu, Ch. Ocena oporów przepływu w terenach zalewowych rzeki Widawy, praca zbiorowa pod redakcją W. Parzonki.

Mokwa, M., Tymków, P., 2004. Koncepcja zastosowania sieci neuronowych w klasyfikacji pokrycia terenu na zdjęciach lotniczych dla potrzeb oceny oporów

przepływów wielkich wód. No. XXII (500) in Zeszyty Naukowe AR Wrocław, Geodezja i Urządzenia Rolne XXII. pp. 25–31.

Mularz, S., 2004. Podstawy teledetekcji. Wprowadzenie do GIS. Wydawnictwo PK.

Nachlik, E., 2000. Metodyka wyznaczania stref zagrożenia powodziowego. Kraków, opracowanie na zlecenie Biura Koordynacji Projektu Banku Światowego.

Parey, P., 1991. Dvwk–merkeblätter 220 zur wasserwirtschaft, hydraulische gerechnung von fliessgewässern. Tech. rep.

Parzonka, W., Radczuk, L., Eliasiewicz, R., Mokwa, M., 2000. Modelling of the flood passage through wroclaw hydrotechnic system. No. 9 vol.1 in Kassel Reports of Hydraulik Engineering, Geodesia et Descriptio Terrarum.

Petryk, S., Bosmajian, G., 1975. Analysis of flow through vegetation, 871–883.

Puzyrewski, R., Sawicki, J., 2000. Podstawy mechaniki płynów i hydrauliki, wyd. II. PWN, Warszawa.

Radczuk, L., Szymkiewicz, R., Jełowicki, J., Żyszkowska, W., Brun, J., 2001. Wyznaczanie stref zagrożenia powodziowego. Oficyna Wyd. READ ME w Łodzi.

Rickert, K., 1986. Der einfluss von geholzen auf abflussverhalten in fliessgewassern. mitteilungen. Tech. Rep. Heft 61, Institunt fur Wasserwirtschaft, Hydrologie und Landwirtschaftlichen Wasserbau der universitat Hannover.

Ripley, B., 1996. Pattern Recognition and Neural Networks. Cambridge Uniwersity Press.

Rutkowski, L., 2005. Metody i techniki sztucznej inteligencji: inteligencja obliczeniowa. Wydawnictwo Naukowe PWN, Warszawa.

Shapiro, L. G., Stockman, G. C., 2001. Computer Vision. Prentice-Hall Inc., New Jersey, USA.

Sobota, J., 1994. Hydraulika tom I i II. Wydawnictwo Akademii Rolniczej we Wrocławiu.

Song, J., Han, S., Kim, Y., 2002. Assessing the possibility of land-cover classification using lidar intensity data. International Archives of Photogrammetry and Remote Sensing, Graz Vol. XXXIV/3B, 259–262.

Straub, C., Weinacker, H., Diedershagen, O., Koch, B., 2006. Standwise delineation based on 3-d information from lidar. Workshop on 3D Remote Sensing in Forestry, 14-15 February, Veinna, Austria. pp. 243–247.

Tadeusiewicz, R., 1993. Sieci neuronowe. Akademicka Oficyna Wydawnicza, Warszawa.

Tadeusiewicz, R., Flasiński, M., 1991. Rozpoznawanie obrazów. Wydawnictwo Naukowo-Techniczne, Warszawa.

Tymiński, T., 1996. Wybrane metody obliczania przepustowości koryt wielodzielnych z uwzględnieniem elementów roślinnych część 1 i 2. No. 301 in Zeszyty Naukowe Akademii Rolniczej we Wrocławiu, Inżynieria Środowiska VIII. Wrocław, pp. 226–253.

Tymków, P., Borkowski, A., 2006. Wykorzystanie danych lotniczego skaningu laserowego do nadzorowanej klasyfikacji pokrycia terenu dla potrzeb modelowania hydrodynamicznego. Archiwum Fotogrametrii, Kartografii i Teledetekcji 16.

Tymków, P., Mokwa, M., 2005. Contemporary methods of the flood flows hydro-

dynamic modelling. No. XXII (500) in XIV International School of Hydraulics. Debrzyno, pp. 169–174.

Tymków, P., Mokwa, M., Borkowski, A., Gołuch, P., 2006. Automatyczna estymacja wartości współczynników oporów przepływu wód w dolinach rzek z wykorzystaniem danych skaningu laserowego oraz zdjęć lotniczych. Problemy Hydrotechniki. Złotniki Lubańskie, pp. 355–362.

Vonk, E., Jain, L., Johnson, R., 1997. Automatic generation of neural network architecture using evolutionary computation. Tech. rep.

Warmink, J., Middelkoop, H., Straatsma, M., 2006. Measuring hydrodynamic vegetation density in a floodplain forest using terrestrial laser scanning. Workshop on 3D Remote Sensing in Forestry, 14–15 February, Veinna. pp. 55–62.

Żelazo, J., 2002. Podstawy renaturyzacji rzek. Wydawnictwo SGGW Warszawa.

Żurada, J., Barski, M., Jędruch, W., 1992. Sztuczne sieci neuronowe. Wydawnictwo Naukowe PWN, Warszawa.

APPLICATION OF PHOTOGRAMMETRIC AND REMOTE SENSING METHODS FOR IDENTIFICATION OF RESISTANCE COEFFICIENTS OF HIGH WATER FLOW IN RIVER VALLEYS

S u m m a r y

This paper focused on remote sensing, photogrammetric, digital acquisition and digital processing methods for the purpose of surface roughness evaluation of floodplains. It presents the technique of automatic identification of land cover for the need of evaluation of resistance coefficients of flood waters on the floodplains using the method of computer-aided decision making and transformation of the obtained coefficients to a hydrodynamic model. Chapter 1 of this publication is an attempt to summarize the literature concerning issues of hydrodynamic calculations and determination of flood hazard zones with respect to the role and methods of flow resistance evaluation. Due to the purpose and nature of this publication, this knowledge is crucial to learn and understand the needs of experts who work in this field. Chapter 2 concerns classification in remote sensing, particularly new techniques and solutions. A method of automatic identification of land cover classes for the need of hydraulic features evaluation of floodplains is also discussed here. The potential sources of data for this classification and the accepted method of accuracy assessment were also indicated. Chapter 3 provides a description of the adopted identification method in the selected part of the river valley, short description of the study area, a discussion of possible approaches to classification as well as an analysis of the results obtained and their accuracy evaluation. Chapter 4 is a summary.

ZASTOSOWANIE METOD FOTOGRAMETRYCZNYCH I TELEDETEKCYJNYCH DO IDENTYFIKACJI WSPÓŁCZYNNIKÓW OPORU PRZEPŁYWU WIELKICH WÓD W DOLINACH RZEK

Słowa kluczowe: współczynniki oporu przepływu, teledetekcja, klasyfikacja nadzorowana, skaning laserowy, modelowanie hydrodynamiczne

S t r e s z c z e n i e

W obliczeniach hydraulicznych rozpatrując dolinę rzeki w czasie przejścia fali wezbraniowej jako pewien system fizyczny, niezbędne jest określenie stanu tego systemu, jego zmiennych charakterystycznych oraz reakcji na oddziaływania zewnętrzne. W celu określenia tych własności systemu fizycznego modeluje się pewną abstrakcję matematyczną. Ze względu na znaczenie gospodarcze terenów zalewowych oraz konsekwencje wezbrań modelowanie przepływów w dolinach jest ważnym działem hydromechaniki i hydrauliki. Prace nad wyznaczaniem stref zagrożenia powodziowego oraz metodami ograniczania skutków powodzi nabrały szczególnego znaczenia po kataklizmach z 1997 i 1998 r. (Kubrak and Nachlik, 2003; Radczuk et al., 2001; Grocki and Czamara, 2001).

Dolina rzeki jako obszar przepływu charakteryzuje się wysoką różnorodnością pokrycia terenu, które ma zasadniczy wpływ na szorstkość powierzchniową. Szczególnie zagospodarowanie rolnicze doliny (grunty orne, łąki i pastwiska), roślinność niska (krzewy) i wysoka (skupiska drzew, lasy) mają różne odzwierciedlenie w oporze przepływu. Parametryzacja wybranych cech geometrycznych roślin odbywa się poprzez określenie rodzaju roślinności (zwłaszcza wysokiej - drzewa liściaste, drzewa iglaste) oraz ich wysokości (Mokwa, 2003). Znajomość tych parametrów pozwala na oszacowanie danych charakterystycznych dla klas szorstkości powierzchniowej takich jak rozstaw drzew, grubość pni itp. W obliczeniach hydraulicznych wartość współczynników oporu można dobierać na podstawie obliczeń tarujących model (Parzonka et al., 2000). Wymaga to między innymi pomiarów hydrometrycznych parametrów hydraulicznych (rozkład prędkości w przekroju), co nie zawsze jest możliwe, zwłaszcza w przypadku przejścia fali wezbraniowej. Innym stosowanym podejściem jest określenie wartości współczynników szorstkości na podstawie analizy kształtu i pokrycia obszaru. Do tego celu wykorzystywane są mapy, zdjęcia lotnicze, bazy danych GIS oraz bezpośrednie pomiary terenowe. Najczęściej stosowaną metodą identyfikacji i klasyfikacji obrazów na zdjęciach lotniczych jest interpretacja wizualna zwana fotointerpretacją (Ciołkosz et al., 1999). Rozwój nowych technik pomiarowych, takich jak skaning laserowy, oraz zaawansowanych numerycznych metod rozwiązywania problemu klasyfikacji, jak np. sieci neuronowe stał się motywacją do sformułowania tezy, że możliwe jest zastosowanie

tych metod do oceny form pokrycia terenów zalewowych uwzględniającej opory przepływu.

Niniejsza praca jest wynikiem kilku lat badań nad teledetekcyjnymi, fotogrametrycznymi i numerycznymi metodami akwizycji i przetwarzania danych dla potrzeb oceny szorstkości powierzchniowej terenów zalewowych. Przedstawiono w niej metodykę automatycznej identyfikacji pokrycia terenu na potrzeby oceny współczynników oporu przepływów wód wezbraniowych na terenach zalewowych za pomocą metod komputerowego wspomagania decyzji oraz transformacji opracowanych współczynników do modelu hydrodynamicznego. Rozdział 1 stanowi próbę podsumowania studiów literaturowych autora nad problemami związanymi z obliczeniami hydraulicznymi oraz wyznaczaniem stref zagrożenia powodziowego w zakresie roli i sposobów oceny oporów przepływu. Ze względu na charakter i cel pracy wiedza ta jest niezbędna do lepszego poznania i zrozumienia potrzeb specjalistów zajmujących się tą tematyką. Rozdział 2 poświęcony jest problematyce klasyfikacji w teledetekcji, w szczególności nowym technologiom i rozwiązaniom z tego zakresu. Przedstawiono tu także metodologię automatycznej identyfikacji klas pokrycia terenu na potrzeby oceny właściwości hydraulicznych terenów zalewowych. W rozdziale tym wskazano potencjalne źródła danych dla takiej klasyfikacji, a także przyjętą metodykę oceny jej dokładności. Rozdział 3 zawiera opis zastosowania przedstawionej metodyki na wybranym fragmencie doliny rzeki, krótką charakterystykę obiektu badawczego, dyskusję nad możliwymi do zastosowania podejściami klasyfikacji a także analizę otrzymanych wyników i ocenę ich dokładności. W rozdziale 4 zawarto podsumowanie pracy.

Appendix

Tab. 1. Visualization of the training set

Class	1			Energy	Entropy	Contrast	2	ASM	Similar.	Disim.	3	4	5
	R	G	B				MAX				DM	INT	LEV
1													
2													
3													
4													
5													
6													
7													
8													
9													
10													
11													
12													
13													
14													

Tab. 2. Visualization of the test set

Tab. 3. Compilation of classification results for the testing set in case of different mask sizes and average GLCM parameters

No	Texture	Reference image	Classification result			
			7×7	15×15	25×25	35×35
K 1						
K 2						
K 3						
K 4						
K 5						
K 6						
K 7						
K 8						
K 9						
K 10						
K 11						
K 12						
K 13						
K 14						

Tab. 4. Compilation of classification results for the testing set in case of different mask sizes and non-average GLCM parameters

No	Texture	Reference image	Classification result			
			7×7	15×15	25×25	35×35
K 1						
K 2						
K 3						
K 4						
K 5						
K 6						
K 7						
K 8						
K 9						
K 10						
K 11						
K 12						
K 13						
K 14						

Tab. 5. Aerial images, patterns and recognition results for classes 15, 16 and 17 – training set
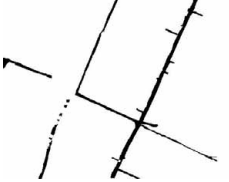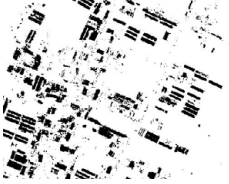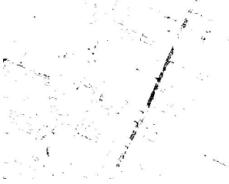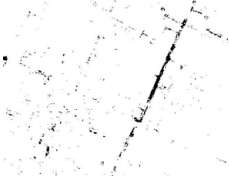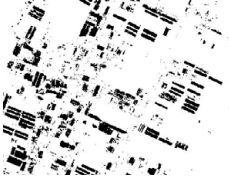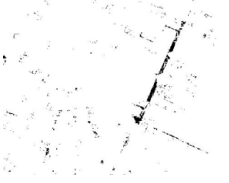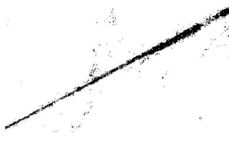
	K15 buildings	K16 roads	K17 railways
image			
pattern			
mask 7x7			
mask 15x15			
mask 25x25			
mask 35x35			

Tab. 6. Aerial images, patterns and recognition results for classes 15, 16 and 17 – test set
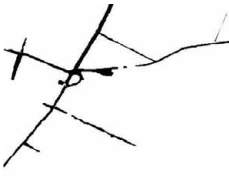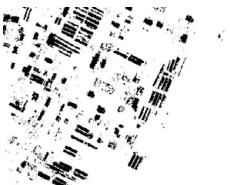
	K15 buildings	K16 roads	K17 railways
image			
pattern			
mask 7x7			
mask 15x15			
mask 25x25			
mask 35x35			

Tab. 7. Compilation of quality measures for the testing set in case of different mask sizes and average GLCM parameters

Class	Mask size$i$	Measure			
		$\hat{\kappa}$	u_i	p_i	d
1	7×7	0.55645	0.41880	0.92328	0.95600
	15×15	0.81072	0.72120	0.95650	0.97774
	25×25	0.91844	0.86400	0.99265	0.98983
	35×35	0.99590	0.99400	0.99839	0.99946
2	7×7	0.52264	0.41080	0.81186	0.95111
	15×15	0.73471	0.59960	0.99734	0.97129
	25×25	0.76660	0.63880	1.00000	0.97420
	35×35	0.90371	0.83480	1.00000	0.98820
3	7×7	0.05960	0.05320	0.21875	0.91880
	15×15	0.10114	0.08280	0.29487	0.92034
	25×25	-0.00830	0.00000	0.00000	0.92420
	35×35	0.00000	0.00000	0.00000	0.92854
4	7×7	0.44350	0.37760	0.63356	0.93995
	15×15	0.39977	0.29320	0.76275	0.94300
	25×25	0.75854	0.72440	0.83226	0.96989
	35×35	0.70067	0.56920	0.96671	0.96783
5	7×7	0.06881	0.09560	0.15765	0.89891
	15×15	0.23591	0.36840	0.25379	0.87751
	25×25	0.14388	0.23240	0.19277	0.87566
	35×35	0.15207	0.20040	0.22012	0.89217
6	7×7	0.04759	0.06960	0.13953	0.90289
	15×15	0.11445	0.14040	0.20336	0.89931
	25×25	-0.06305	0.00000	0.00000	0.87786
	35×35	-0.05923	0.00000	0.00000	0.88263
7	7×7	0.13088	0.12400	0.27003	0.91349
	15×15	0.01956	0.02440	0.13319	0.91897
	25×25	0.25722	0.16480	0.82731	0.93789
	35×35	0.03007	0.02040	0.32075	0.92694
8	7×7	0.65547	0.75280	0.62401	0.94994
	15×15	0.73433	0.74080	0.76561	0.96529
	25×25	0.64557	0.75360	0.60892	0.94783
	35×35	0.66457	0.72800	0.65538	0.95323
9	7×7	0.97906	1.0000	0.96191	0.99717
	15×15	0.99024	0.98360	0.99838	0.99871
	25×25	0.95518	0.92280	0.99654	0.99426
	35×35	0.99145	1.00000	0.98425	0.99886
10	7×7	0.96002	0.99880	0.92963	0.99451
	15×15	0.99102	1.00000	0.98348	0.99880
	25×25	0.99978	1.00000	0.99960	0.99997
	35×35	0.99784	0.99760	0.99840	0.99971

Tab. 8. Compilation of quality measures for the testing set in case of different mask sizes and average GLCM parameters − continued

Class	Mask size$i$	Measure			
		$\hat{\kappa}$	u_i	p_i	d
11	7×7	0.55325	0.79040	0.47466	0.92254
	15×15	0.56234	0.85080	0.46665	0.91989
	25×25	0.70792	0.90720	0.61463	0.95274
	35×35	0.93865	0.91120	0.97684	0.99211
12	7×7	0.71865	0.77760	0.70537	0.96091
	15×15	0.85906	0.96320	0.79341	0.97946
	25×25	0.98565	0.97680	0.99673	0.99811
	35×35	0.90094	0.98360	0.84415	0.98586
13	7×7	0.97355	0.98560	0.96552	0.99646
	15×15	0.83626	0.99840	0.73956	0.97477
	25×25	0.78961	0.96120	0.69551	0.96717
	35×35	0.80848	0.98080	0.71093	0.97014
14	7×7	0.92832	0.96160	0.90717	0.99023
	15×15	0.34746	0.29800	0.52837	0.93086
	25×25	0.22972	0.22080	0.35407	0.91557
	35×35	0.36627	0.54200	0.34496	0.89377
15	7×7	0.90615	0.98075	0.91207	0.90613
	15×15	0.90873	0.97811	0.91637	0.90832
	25×25	0.90937	0.97774	0.91726	0.90889
	35×35	0.90927	0.97743	0.91738	0.90877
16	7×7	0.96038	0.99801	0.96175	0.95998
	15×15	0.96101	0.99676	0.96337	0.96051
	25×25	0.96021	0.99782	0.96174	0.95980
	35×35	0.96008	0.99795	0.96151	0.95968
17	7×7	0.95949	0.96091	0.99654	0.95841
	15×15	0.97251	0.97935	0.99236	0.97237
	25×25	0.97843	0.98628	0.99172	0.97847
	35×35	0.97987	0.98854	0.99099	0.97996

Tab. 9. Compilation of quality measures for the testing set in case of different mask sizes and non-average GLCM parameters

Class	Mask size$i$	Measure			
		$\hat{\kappa}$	u_i	p_i	d
1	7×7	0.75079	0.71480	0.82808	0.96903
	15×15	0.97015	0.95240	0.99291	0.99611
	25×25	0.97530	0.97080	0.98339	0.99674
	35×35	1.00000	1.00000	1.00000	1.00000
2	7×7	0.71354	0.62400	0.88086	0.96711
	15×15	0.81210	0.70320	0.99266	0.97843
	25×25	0.92675	0.87200	1.00000	0.99086
	35×35	0.99698	0.99440	1.00000	0.99960
3	7×7	0.08533	0.07800	0.23839	0.91634
	15×15	0.22874	0.16880	0.52553	0.92974
	25×25	0.05497	0.04280	0.26551	0.92317
	35×35	-0.00286	0.00000	0.00000	0.92711
4	7×7	0.27866	0.24720	0.43737	0.92351
	15×15	0.50795	0.39680	0.80324	0.94997
	25×25	0.86043	0.79680	0.95677	0.98291
	35×35	0.89463	0.82320	0.99613	0.98714
5	7×7	-0.01784	0.02200	0.04538	0.89709
	15×15	0.22289	0.35960	0.24193	0.87377
	25×25	0.27622	0.55440	0.25278	0.85111
	35×35	0.28623	0.67160	0.24666	0.83003
6	7×7	0.28427	0.25160	0.44421	0.92406
	15×15	0.06426	0.10200	0.14448	0.89271
	25×25	-0.01634	0.00000	0.00000	0.91951
	35×35	-0.00928	0.00000	0.00000	0.92366
7	7×7	0.73066	0.68560	0.82325	0.96703
	15×15	0.93287	0.90600	0.97127	0.99137
	25×25	0.97762	0.97000	0.98858	0.99706
	35×35	0.99246	0.99320	0.99280	0.99900
8	7×7	0.66136	0.72600	0.65171	0.95271
	15×15	0.62406	0.58680	0.72373	0.95449
	25×25	0.68540	0.66040	0.75908	0.96077
	35×35	0.74369	0.62560	0.96187	0.97148
9	7×7	0.99039	1.00000	0.98232	0.99871
	15×15	0.99571	0.99960	0.99245	0.99943
	25×25	0.98827	1.00000	0.97847	0.99843
	35×35	0.99871	1.00000	0.99761	0.99983
10	7×7	0.96446	0.99880	0.93731	0.99514
	15×15	0.97192	0.99520	0.95362	0.99620
	25×25	0.94057	0.99720	0.89805	0.99171
	35×35	0.98440	0.99400	0.97719	0.99791

Tab. 10. Compilation of quality measures for the testing set in case of different mask sizes and non-average GLCM parameters – continued

Class	Mask sizei	Measure			
		$\hat{\kappa}$	u_i	p_i	d
11	7×7	0.78410	0.97800	0.68011	0.96557
	15×15	0.98864	0.99480	0.98417	0.99849
	25×25	0.97595	1.00000	0.95639	0.99674
	35×35	0.96147	1.00000	0.93110	0.99471
12	7×7	0.74475	0.85360	0.69286	0.96251
	15×15	0.93114	0.99120	0.88721	0.99037
	25×25	0.99114	0.98800	0.99557	0.99883
	35×35	0.99265	0.98880	0.99758	0.99903
13	7×7	0.95023	0.95800	0.94964	0.99337
	15×15	0.83351	0.95600	0.75994	0.97529
	25×25	0.62491	0.71480	0.60270	0.94597
	35×35	0.72275	0.90920	0.63262	0.95580
14	7×7	0.82642	0.76000	0.93274	0.97894
	15×15	0.71512	0.64160	0.85365	0.96654
	25×25	0.57326	0.46320	0.83190	0.95497
	35×35	0.56534	0.59200	0.60041	0.94271